On the Seasonal Cycle of Phytoplankton Bio-Optical Properties Inside a Warm Core Ring in the Gulf of Mexico

Amaru Márquez-Artavia[1], Enric Pallàs-Sanz[1], M. Tenreiro[1]

[1]Grupo de Monitoreo Oceanográfico con Gliders. Centro de Investigación Científica y de Educación Superior de Ensenada, Baja California

Key Points:

- Optical data suggest changes in the phytoplankton taxonomic composition along a seasonal cycle.
- The seasonal cycle explains most of the variability of bio-optical properties near the eddy core.
- The entrainment of nutrients into the euphotic zone during winter supports the seasonal signal of phytoplankton biomass.

Corresponding author: Amaru Márquez-Artavia, Enric Pallàs-Sanz, `amaru@cicese.mx`, `epallas@cicese.mx`

Abstract

Four underwater glider missions were carried out to sample the physical and bio-optical properties inside a Loop Current Eddy (LCE) in the Gulf of Mexico (GoM), to investigate whether the winter deepening of the mixed-layer and erosion of the nitracline stimulates phytoplankton growth. Recent coupled physical-biogeochemical numerical models support this mechanism, but observations using Lagrangian floats suggest that there is no seasonal cycle on integrated phytoplankton biomass. Here, data collected by underwater gliders during a full seasonal cycle and inside the LCE Poseidon support the occurrence of a seasonal cycle, which is consistent with nutrient entrainment into the euphotic zone. The changes in fluorescence emission per chlorophyll-a unit and its implications for interpreting bio-optical variability were also assessed. Linear regressions between *in vivo* chlorophyll-a fluorescence and satellite chlorophyll-a concentration show the largest (smallest) slopes during winter (summer), suggesting a shift in the phytoplankton community along the year. Although the glider dataset is convolved by temporal and spatial variability, and chlorophyll-a fluorescence is affected by several factors, the concomitant enhancement of particle backscattering coefficient and chlorophyll-a observed during winter supports the occurrence of a seasonal cycle in phytoplankton biomass. Deep winter convection inside the core of the LCE, can promote fertilization through vertical diffusion of nutrients. Poseidon was an extraordinary, large, and strong, LCE that prompted phytoplankton blooms in winter highlighting their relevance for primary production and in general for biogeochemical processes.

Plain Language Summary

Recent technological advancements have revolutionized our ability to monitor changes in the primary producers of the sea. Specialized robots are nowadays capable of measuring bio-optical properties, such as chlorophyll-a fluorescence and the particle backscattering coefficient even during severe climate conditions. However, interpreting chlorophyll-a fluorescence measurements can be challenging, as they are influenced by multiple factors, including phytoplankton community shifts, and nutritional status. Here, we used data acquired by remotely controlled platforms to track a large coherent rotating oceanic eddy as it propagated westward through the Gulf of Mexico. Near the center of the eddy, the upper 170 meters of the water column were mixed thoroughly by strong winds during winter, redistributing particles from deeper layers towards the upper ones including nutrients required for phytoplankton growth. The dataset revealed a correlation between the strong winter mixing and an increase in both, the chlorophyll-a concentration and particle backscattering. Therefore, nutrient injection stimulated phytoplankton growth during winter. We also found that fluorescence per chlorophyll-a concentration changes dramatically during the year, presumably because the types of phytoplankton shift along the seasons. Observed high-frequency phytoplankton response to winds in this dataset is still to be analyzed and will be the basis for future work.

1 Introduction

Seasonal variability of wind speed and turbulent heat fluxes at the sea surface modulate the Mixed Layer Depth (MLD), which ultimately plays a key role in regulating the light and nutrient availability for the phytoplankton (Mann & Lazier, 2006). According to Sverdrup's hypothesis, the critical depth is a horizon defining the maximum depth that the MLD can reach before causing a light limitation for a net phytoplankton population growth. For example, in the North Atlantic and some regions of the Mediterranean Sea, winter convection deepens the mixed layer down to the depth of the nitracline, promoting nutrient injection into the euphotic zone. Eventually, the MLD becomes deeper than critical depth, reducing the light availability, and delaying the onset of the phytoplank-

ton bloom until the spring, when the MLD restratifies (Sverdrup, 1953; Lavigne et al., 2013; Mignot et al., 2018).

The phenology of phytoplankton blooms can differ from the classical North Atlantic bloom. Maximum phytoplankton biomass also occurs in phase with the MLD during winter, in the so-called entrainment blooms (Cullen et al., 2002). In this scenario, the MLD is shallower than the critical depth, the light does not become a limiting factor, and phytoplankton growth is supported by the injection of new nutrients during the winter deepening of the mixed layer. Entrainment blooms are thought to explain the seasonal cycle of phytoplankton in the Gulf of Mexico (GoM) based on satellite-derived sea surface chlorophyll-a. Maximum values are observed during winter and minimum values are observed during summer (Muller-Karger et al., 1991, 2015).

In recent years, the annual seasonal cycle of phytoplankton biomass in the GoM has been questioned. Pasqueron et al. (2017), using Lagrangian floats show constant depth-averaged chlorophyll-a concentration along the year in the GoM, suggesting that winter convection only redistributes the phytoplankton cells from the deep chlorophyll-a maximum (DCM) towards the surface. Certainly, this process can increase the pigment concentration at the surface but, in an average sense, the phytoplankton biomass remains constant. Therefore, enhancement of surface chlorophyll-a is not necessarily related to a net phytoplankton growth within the euphotic layer. In this respect, results from coupled physical and biogeochemical numerical models have shed light reconciling both views (i.e. redistribution versus enhancement of phytoplankton biomass).

Damien et al. (2018) suggest that the distance between the MLD and the nitracline varies regionally in the GoM, and it is a key variable in determining if either a redistribution of chlorophyll-a or an increase on the integrated phytoplankton biomass drives the Gulf's seasonal cycle. The authors found that in regions where the MLD and the nitracline are close or overlap, nutrients are injected into the euphotic zone, causing an increase in the phytoplankton biomass. Conversely, when the MLD is shallower than the nitracline, the DCM is redistributed within the mixing layer. Moreover, Damien et al. (2021) shows that the MLD frequently reaches the nitracline inside Loop Current Eddies (LCEs) because stratification is weaker, producing deeper mixed layers. That is, it is required less momentum input inside the LCE to mix the water column to the depth of the nitracline ($\sim$ 180 m in average inside LCEs; 140m outside; Portela et al. (2018)).

LCEs are important because not only drive the GoM's mesoscale circulation but, also shape the distribution of physical, chemical, and biological properties (Meunier, Pallás-Sanz, et al., 2018; Portela et al., 2018; Lee-Sánchez et al., 2022; Linacre et al., 2015, 2019; Damien et al., 2021). Inside these mesoscale eddies, vertical pumping of nutrients into the euphotic layer (Falkowski et al., 1991; McGillicuddy & Robinson-F, 1997; McGillicuddy et al., 1998; McGillicuddy, 2016; Siegel et al., 2011) and changes in the Photosynthetically Active Radiation (Vaillancourt et al., 2003) are important factors controlling the heterogeneity of chlorophyll-a concentration. The nature of oceanic pumping is diverse (Klein & Lapeyre, 2009), including frictional decay (P. J. S. Franks et al., 1986; Flierl & Mied, 1985), linear and non-linear Ekman pumping (Ekman, 1905; Stern, 1965; Wenegrat & Thomas, 2017; Chen et al., 2020), eddy-wind interaction (McGillicuddy et al., 2007; Gaube et al., 2013; Martin & Richards, 2001), and horizontal strain deformation (Hoskins et al., 1978; Pallàs-Sanz & Álvaro Viúdez, 2005; Barceló-Llull et al., 2017; Estrada-Allis et al., 2019). Moreover, different processes can be at work simultaneously. For instance, He et al. (2017) found that coupled eddy-induced Ekman pumping and winter mixing is a robust physical mechanism to explain phytoplankton blooms inside the mixed layer of anticyclonic eddies.

In the GoM, the role of light on the seasonal cycle of the phytoplankton has been formally assessed only in the work of Yang et al. (2022) who implemented a diagnostic model to compute the net primary production based on *in situ* estimations of phytoplank-

Table 1. General information of the glider missions designed to sample the Poseidon LCE in the GoM. It includes the mission number, number of dive cycles done during the whole mission, start date and end date of each mission, the Eco WETlabs triplet (BBFL2IRB) serial numbers, and their corresponding scale factor (SF) reported by the manufacturer in the calibration sheet.

Mission	Dive cycles	Start date	End date	BBFL2 SN	SF $[mg\,\mathrm{count}^{-1}]$
0003	625	05-08-2016	15-11-2016	1374	0.0121
0004	639	07-12-2016	29-03-2017	1374	0.0121
0005	711	10-02-2017	25-05-2017	1375	0.0121
0006	507	25-05-2017	22-08-2017	1376	0.0121

ton carbon. They found that the net primary production integrated in the upper 100 m is higher during the summer and lower during winter, because of the seasonal cycle of irradiance in the GoM. This highlights the lack of consensus on the factors controlling phytoplankton growth and primary productivity in the GoM. Especially inside deep water LCEs (> 1000 m depth), where different mechanisms can affect the phytoplankton communities dominated by *Prochlorococcus* cells (Linacre et al., 2015, 2019), adapted to proliferate in oligotrophic regions (Partensky et al., 1999; Partensky & Garczarek, 2010; Biller et al., 2014).

Although previous studies have contributed to the understanding of the seasonal cycle of phytoplankton in the GoM, including LCEs dynamics, they are also limited in several aspects. Satellite data are constrained to surface waters, while data collected by Lagrangian floats profiling the water column every 14 days can filter out high-frequency processes important for phytoplankton dynamics (Platt et al., 1989; Lewis et al., 1984; P. J. Franks, 2015; Taylor & Ferrari, 2011). On the other hand, the results of numerical modeling require validation with *in situ* measurements, especially during winter and inside the eddy core, where the lack of observations reduces the skill of the model in simulating realistic vertical profiles of chlorophyll-a (Damien et al., 2018, 2021). Here a full seasonal cycle of bio-optical properties inside a westward propagating LCE is investigated, by using a combination of high-resolution and quality-controlled, measurements of hydrography, *in vivo* chlorophyll-a fluorescence, and particle backscattering.

2 Data and Methods

Four underwater glider missions (Table 1) were designed to sample a LCE called Poseidon, that propagated through the GoM between 2016 and 2017 (Figure 1). Gliders sampled the water column from the surface up to 1000 m depth in a saw-tooth pattern, with a suite of sensors to simultaneously measure physical and biogeochemical properties. The sensors used were: unpumped CT-Sail (temperature and conductivity), an optode Aanderaa 4831 (dissolved oxygen), and the ECO-Wetlabs triplet (BBFL2IRB; Table 1) which measures light backscattering (at 700 nm and with a centroid angle of 124°), *in vivo* fluorescence of chlorophyll-a (ex: 470 nm, em: 695 nm), and fluorescence emitted from colored dissolved organic matter (ex: 370 nm, em: 460 nm). During mission 3, the ECO-Wetlabs triplet was turned off below 200 m to reduce the glider's battery consumption. For calibration purposes, two dive cycles were performed down to dark and deep waters of 1000 m depth.

A glider dive cycle includes measurements collected during the downcast and upcast, with horizontal and time resolution at the surface of 4 km and 6 hours, respectively. The averaged vertical resolution was 0.6 m for the physical variables and 1 m for the biogeochemical sensors. TEOS-10 equation of seawater was used to compute density anomaly

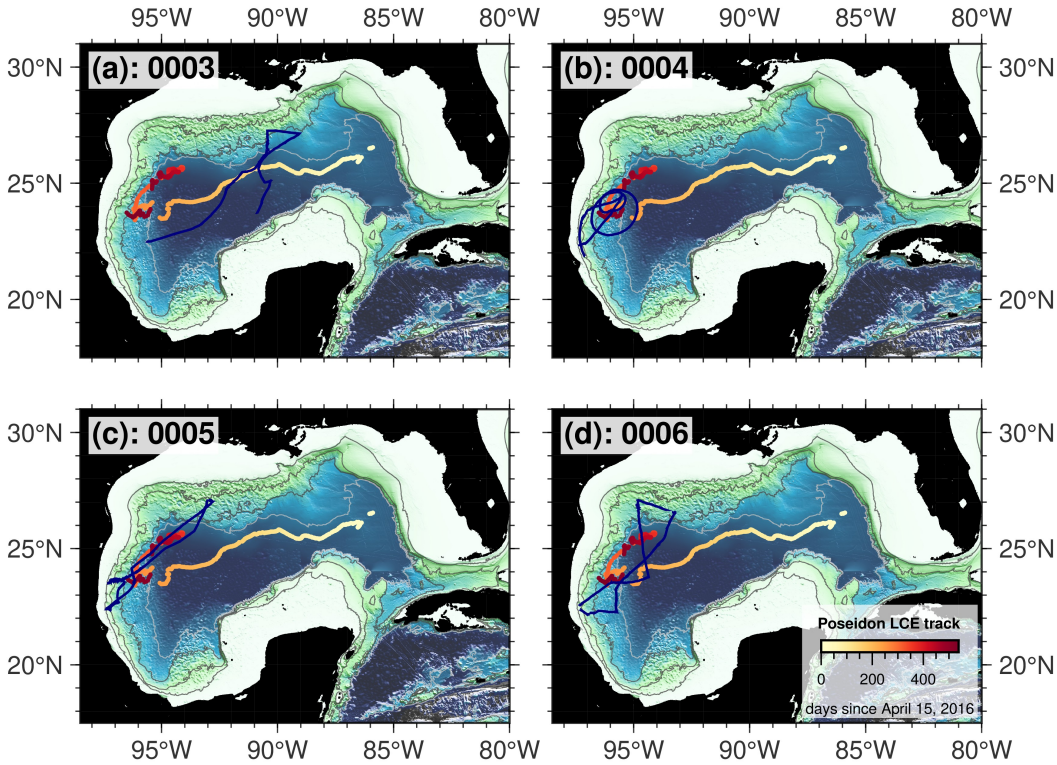

Figure 1. The trajectory of the LCE Poseidon and the paths followed by underwater gliders during the four missions. Glider's trajectories for each mission (see Table 1) are represented by the blue line, while the Poseidon track is color-coded based on the days since its detachment from the Loop Current (April 15, 2016; Meunier, Pallás-Sanz, et al. (2018)). Background colors (blue to white) represent the bathymetry of the GoM, and the contours of the 200, 500, 1000, 2000, and 3000 m are shown. Note the sampling pattern of the glider during mission 4, which was produced by the glider drifting with the Poseidon depth-averaged currents.

referred to the surface. Squared Brunt-Väisälä frequency and the MLD were derived from potential density anomaly. The MLD was determined as the depth at which density exceeds a threshold of $0.125\,\mathrm{kg\,m^{-3}}$ relative to the value recorded near the surface (i.e. 10 m depth).

The particle backscattering coefficient at 700 nm ($b_{bp}700$) was obtained following Schmechtig, Poteau, et al. (2018), after removing the contribution of seawater. It was quality controlled following Argo data processing (Schmechtig et al., 2019). The chlorophyll-a concentration from fluorescence was obtained by subtracting the dark counts (i.e., the blank or the signal of the fluorometer in the absence of chlorophyll-a) and by using a scale factor (SF), that is, ($[Chl_a] = (Fl_{raw} - \mathrm{dark\,counts}) \cdot SF$). Even though the manufacturer provides the calibration coefficients, it is important to note that they might exhibit deviations from one sensor to another, and during the field mission. Here, the *in situ* dark count coefficient was obtained by averaging the deepest observations of fluorescence (below the euphotic layer), a procedure used by the Argo-BGC program (Schmechtig, Claustre, et al., 2018).

In this study, two scale factors were used to convert fluorescence into chlorophyll-a concentration: (i) from the calibration sheet provided by the manufacturer (Table 1), and (ii) an adjusted scale factor inferred from the linear fit between the satellite-derived chlorophyll-a concentration and the glider's fluorescence. On one hand, the adjusted scale factor is used to assess the relation between fluorescence and chlorophyll-a concentration, and on the other hand, it attempts to reduce bias in the chlorophyll-a estimation along the seasonal cycle.

The non-photochemical quenching correction on chlorophyll-a fluorescence was done according to the methodology described in Thomalla et al. (2018), which takes advantage of the high spatio-temporal resolution of gliders, and the relation between chlorophyll-a and $b_{bp}700$. This procedure interpolates vertically and removes anomalous spikes from chlorophyll-a and $b_{bp}700$ data. High-frequency variability in chlorophyll-a was removed by applying a 7-point running mean with a Hann window. All points exceeding three times the standard deviation were considered spikes. The $b_{bp}700$ de-spiked signal is in agreement with the baseline described in Briggs et al. (2011).

2.1 Relation between glider *in situ* fluorescence and satellite chlorophyll-a concentration

Changes in the relation between fluorescence and extracted chlorophyll-a are a function of phytoplankton taxonomic composition, nutritional status, and growth phase (Proctor & Roesler, 2010; C. Roesler et al., 2017). Since water samples were not available during the four glider missions, satellite data was used to obtain adjusted scale factors for the region (C. Roesler et al., 2017). The method of Boss et al. (2008), which compares the chlorophyll-a fluorescence with a satellite data product, assumed to be the ground truth, was followed. Night-time fluorescence measurements were only considered to avoid introducing variability related to the correction of non-photochemical quenching.

Here it was used the daily ESA OC-CCI v5 dataset (`ESAOC-CCI;https://climate.esa.int/en/projects/ocean-colour/data/`), with a spatial resolution of $4\,\mathrm{km}\times4\,\mathrm{km}$. In this product, ocean color measurements are obtained from multiple satellite radiometric sensors and merged, reducing artifacts introduced by differences in sensor design (i.e., differences in sampled wavelengths). Also, the algorithm used to retrieve chlorophyll-a concentration from remote sensing reflectance is selected by taking into consideration the optical classification of a water body (Sathyendranath et al., 2019). Moreover, by merging data from multiple sensors, the ESA OC-CCI improves spatial coverage, which is an important advantage in regions frequently covered by clouds like the GoM.

A critical step to establish and interpret relationships between satellite data and *in situ* measurements, is to identify observations that can be properly compared, given the differences in the spatial and temporal resolutions captured by both platforms (Gordon et al., 1983; Bailey & Werdell, 2006; Concha et al., 2021). The procedure to find such observations is called match-up analysis, and there are different approaches. They are not interpolations of the satellite data into the position of field measurements, which can fail due to the presence of clouds, and do not take into account differences in the resolution of different platforms. More details about the match-up analysis can be found elsewhere in the literature (Gordon et al. (1983); Bailey and Werdell (2006); Concha et al. (2021)).

The match-up analysis used here was consistent with the protocols to validate the ESA-OC-CCI product (Sathyendranath et al., 2019; Valente et al., 2019). Briefly, the glider observations of chlorophyll-a fluorescence (in digital counts) within the upper 10 m depth were averaged. The 10 m depth criterion was selected because it is the maximum valid depth to relate *in situ* and satellite data in the ESA OC-CCI products, and it is a compromise between the optical depth in oligotrophic and eutrophic waters (Sathyendranath et al., 2019; Valente et al., 2019). Matched-up satellite observations are obtained as the median of a 3x3 pixel window centered at each glider position. The median value was considered valid only if the central pixel was not affected by clouds. If several glider observations fall inside the 3x3 box, only the nearest to the center was used.

The relationship between the matched pairs was analyzed using a type I linear regression. To account for the auto-correlation of the glider's measurements and the heteroskedasticity, the confidence intervals of the coefficients and best-fit line were adjusted, as recommended by Fox (2016). The slope of this regression was used to estimate the adjusted scale factor for estimating the chlorophyll-a concentration. Outliers were detected by visual inspection of scatter plots and removed accordingly.

2.2 Eddy detection

The center and periphery of the LCE Poseidon were identified by using an algorithm applied over Sea Level Anomalies (SLAs). In this work, the daily SLAs were obtained from the Delayed-Time merged all satellites Global Ocean Gridded SSALTO/DUACS Sea Surface Height, an L4 product available in the Copernicus Marine Service (`https://marine.copernicus.eu/access-data`). Before the use of the eddy detection algorithm, $0.25^\circ \times 0.25^\circ$ gridded data were filtered with a two-dimensional LOESS smoother to attenuate processes with wavelengths greater than 20° in longitude and 10° in latitude (Chelton, Schlax, & Samelson, 2011), that can remove the large scale effects on the sea level like steric effect.

The LCE Poseidon was identified as a closed contour of SLA that meets the following criteria: (i) the SLA closed contour should contain a minimum of 8 pixels, but not more than 1000, (ii) there is at least one local maximum of SLA, (iii) the amplitude of the eddy is greater than 1 cm, and (iv) all pairs of pixels within the contour have distances smaller than a threshold that depends on latitude (for details see Appendix B in Chelton, Schlax, and Samelson (2011)). The outermost closed contour of SLA full-filling the four criteria defines the so-called effective contour of the eddy. A successive search within the effective contour is conducted to find the closed SLA contour with the largest swirl geostrophic speed.

The contour inside the eddy is called the maximum speed contour, and it is a natural border separating the interior of the eddy dominated by vorticity, from external regions dominated by straining. Tracers cannot escape from within the vortical region when diffusion is neglected (Chelton, Schlax, & Samelson, 2011; Meunier, Pallás-Sanz, et al., 2018). This is an important characteristic of nonlinear eddies (Flierl, 1981), that can trap

fluid in their interior for long distances without exchanging fluid with the surrounding waters.

The trajectory of Poseidon was computed by searching for the nearest eddy center (i.e. the centroid of the effective contour) between consecutive days according to Chelton, Schlax, and Samelson (2011). On the other hand, the distance between the glider and the eddy centroid (d) was computed and normalized by the eddy length scale (L). This normalized distance ($R = d/L$) was used to select the vertical profiles inside the core of the eddy ($R < 0.55$), which allows constraining the variability to vertical (1D) processes by neglecting horizontal advection.

The trajectory of the eddy was smoothed using a 1-D LOESS with a half-span of 42 days (Chelton, Schlax, & Samelson, 2011). The time derivative of the smoothed trajectory provides the eddy's translation speed, and the rotational speed of the eddy was computed as the averaged swirl speed along the maximum speed contour. The degree of nonlinearity of the eddy is given by the ratio between rotational and translation speed (Flierl, 1981; Chelton, Schlax, & Samelson, 2011). Rotational and translation speed and the nonlinearity parameter were averaged in $0.5\,^{\circ}$ bins, and were used to describe the kinematical properties of LCE Poseidon along its westward propagation across the GoM.

2.3 Ancillary variables

Two main factors stimulating phytoplankton growth are the nutrient concentration and the amount of Photosynthetically Active Radiation (PAR). Since the gliders do not measure these variables, estimating them from proxies is required. Changes in nutrient availability can be assessed from the distance between the MLD and the nitracline depth (Damien et al., 2018) because entrainment of nutrients can occur when they are close or overlap. Following Pasqueron et al. (2017), the top of the nitracline is equal to the depth of the $25.5\,\mathrm{kg\,m^{-3}}$ isopycnal, which was determined to be the nitrate depletion density (Omand & Mahadevan, 2015).

The $25.5\,\mathrm{kg\,m^{-3}}$ isopycnal can overestimate the depth of the nitracline (see table 4 in Lee-Sánchez et al. (2022)), and other methods can be used as an alternative. For example, it is possible to obtain the depth of the nitracline from reconstructed nitrates plus nitrites ([N+N]) profiles based on hydrographic variables Velásquez-Aristizábal et al. (2022). From these profiles, the nitracline (nitracline-VA22 hereinafter) can be considered the depth where the [N+N] exceed $0.5\,\mu\mathrm{mol\,kg^{-1}}$.

A combination of satellite data products is used to estimate the underwater distribution of PAR (400-700 nm). The datasets used for this purpose were: (i) the previously described ESA OC-CCI to compute the diffuse attenuation coefficient for the PAR ($Kd(PAR)$), and (ii) the EPICS/DISCOVR dataset with a satellite measurement of the daily averaged PAR just above the sea surface ($Ed(0^{+}, PAR)$, R. J. Frouin et al. (2018); R. Frouin et al. (2022)). Both products are daily available but differ in their spatial resolution. ESA-OC-CCI is a 4 km product, while EPICS/DISCOVR is in a regular grid of $18\,\mathrm{km} \times 18\,\mathrm{km}$ (`https://asdc.larc.nasa.gov/`).

The procedure is based on the Lambert-Beer law, which describes the exponential decay of irradiance with depth, given the irradiance reaching the sea surface and the diffuse attenuation coefficient (K_d). Both quantities depend on the wavelength. The interest was to find the depth of an isolume with physiological significance (for a discussion about the depth of the euphotic zone see Letelier et al. (2004) and Banse (2004)), defining the base of the euphotic zone. The attenuation coefficient of the PAR ($Kd(PAR)$) was estimated from the value obtained at the single wavelength of 490 nm ($Kd(490)$), which is only available in the ESA-OC-CCI product. At each pixel the $Kd(PAR)$ was obtained following the relation provided by Morel et al. (2007):

$$Kd(PAR) = 0.0665 + 0.874 \cdot Kd(490) - 0.00121 \cdot Kd(490)^{-1}. \quad (1)$$

Given the presence of clouds in the ESA-OC-CCI dataset, a representative value of $Kd(PAR)$ was used. Similar to the match-up analysis, this value was the median of a 3x3 pixel box centered at each glider position. PAR from the EPICS/DISCVR dataset was interpolated at each glider surface position, taking advantage that does not present data gaps by clouds and because it was not used for comparisons with *in situ* data. The depth of the $0.08\,\mathrm{molQ\,m^{-2}\,day^{-1}}$ isolume was computed by solving the Lambert-Beer law, following to Mignot et al. (2018). This isolume value was selected because is the compensation irradiance for low-light adapted ecotypes of *Prochlorococcus* (Moore et al., 1995), which have been found at the base of the euphotic zone in the GoM (Linacre et al., 2015, 2019). Daily averaged isolume depth was used to study the vertical displacements of the DCM in relation to the seasonal changes in underwater light, similarly as in other studies (Letelier et al., 2004; Mignot et al., 2014).

Phytoplankton light limitation inside LCE Poseidon was assessed through a comparison of the MLD and the Sverdrup's critical depth (Z_{cr}) (Sverdrup, 1953; Siegel et al., 2002; Lavigne et al., 2013), which can be obtained from the relationship given by:

$$\frac{1}{Kd(PAR) \cdot Z_{cr}} \left(1 - e^{-Kd(PAR) \cdot Z_{cr}}\right) = \frac{Ed_c}{Ed(0^+, PAR)} \quad (2)$$

where $Kd(PAR) = 0.075\,\mathrm{m^{-1}}$ is the attenuation coefficient of PAR averaged along the winter mission 0004. $Ed(0^+, PAR)$ is the PAR just above the sea surface, and Ed_c is the community compensation irradiance. $Ed(0^+, PAR)$ was obtained from the EPICS/DISCOVR dataset, and Ed_c was set to $1.1\,\mathrm{molQ\,m^{-2}\,day^{-1}}$ (Regaudie-De-Gioux & Duarte, 2010; Siegel et al., 2002). Z_{cr} was averaged daily.

3 Results

3.1 Relation between fluorescence and satellite chlorophyll-a concentration

In the four missions, there were linear associations between fluorescence and chlorophyll-a (Table 2) as shown in Figure 2. However, the coefficients of the linear model were different from one mission to another (Table 2), as well as their uncertainties, and the amount of explained variance by the linear model (i.e., squared Pearson correlation coefficient, r^2). Winter missions show the highest slopes, but also the highest uncertainties in the model coefficients (Table 2). Mission 0004 shows the largest scattering of values around the predicted line, and consequently, the linear model explains less of the total variance (r^2=0.46; Table 2).

A more complex relation was observed during winter missions (0004 and 0005), which showed the highest uncertainties in the model coefficients and the largest scattering around the best-fit line. This can be associated with the variability of the fluorescence yield, driven by the multiple factors that can affect it such as nutritional status, phytoplankton community composition, and growth phase. All these factors can have a higher spatiotemporal variability during winter, contributing to the total variance and leading to a more scattered distribution of observations (C. S. Roesler & Barnard, 2013).

The relation between chlorophyll-a and fluorescence is thus more convoluted during mission 0004 because the glider sampled the LCE alongstream following a circular pattern, sometimes getting close to the contour of maximum speed (Figure 1b). This suggests that eddy spatial structure may have a role in modulating phytoplankton populations, at least in terms of their fluorescence emission. Some aspects of the spatial dis-

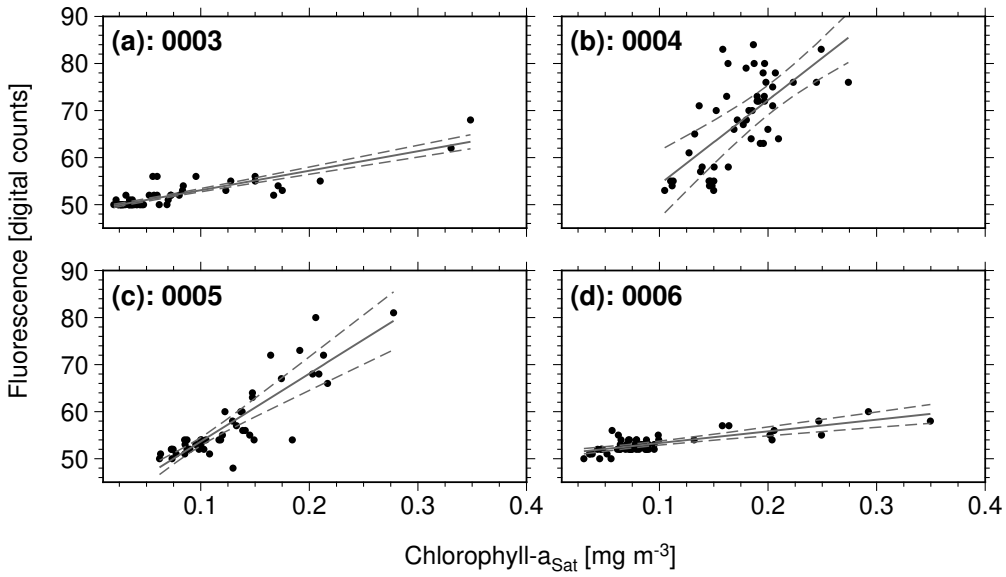

Figure 2. Linear regressions between fluorescence and satellite-derived chlorophyll-a concentration for each glider mission: 0003 (a), 0004 (b), 0005 (c), and 0006 (d). In each panel, the least-squares fitted line and the 95% confidence intervals are shown.

Table 2. Statistics of the linear regressions between glider fluorescence and satellite chlorophyll-a concentration in each mission. N is the number of observations (valid matchups) for the least squares fitting. The slope and intercept of the linear regression are indicated together with coefficient uncertainties. r^2 is the squared Pearson's correlation coefficient.

Mission	N	Slope	Intercept	Pearson's r	r^2
0003	62	41.48 ± 2.57	48.91 ± 0.21	0.88	0.77
0004	50	179.19 ± 30.49	36.38 ± 6.45	0.68	0.46
0005	49	144.51 ± 16.87	39.17 ± 1.71	0.87	0.76
0006	57	24.88 ± 3.66	50.82 ± 0.37	0.80	0.64

tribution and transformation of physical and biological properties across mesoscale eddies have been studied in previous works in the GoM and other locations (Sosa-Gutiérrez et al., 2020; Lee-Sánchez et al., 2022; Damien et al., 2021; Liu et al., 2020; Chelton, Gaube, et al., 2011; Sánchez-Velasco et al., 2013; Peterson et al., 2011; Velásquez-Aristizábal et al., 2022).

Linear regressions indicate changes in the adjusted scale factor (the inverse of the slope reported in Table 2), which varied between 0.006 mg m^{-3} counts^{-1} (mission 0004) to 0.040 mg m^{-3} counts^{-1} (mission 0006). The variation in the scale factor contrasted with the constant value provided by the manufacturer for all missions (0.0121 mg m^{-3} counts^{-1}; Table 1), which can lead to changes in the estimated chlorophyll-a.

Hence, the estimated chlorophyll-a concentration obtained with the manufacturer and adjusted scale factors were compared with satellite chlorophyll-a concentration (Figure 3). Typically, regardless of the scale factor used, the chlorophyll-a concentration at the surface is large (small) during winter (summer) (Figure 3). However, there are discrepancies relative to the satellite data depending on the scale factor used to obtain the chlorophyll-a from fluorescence.

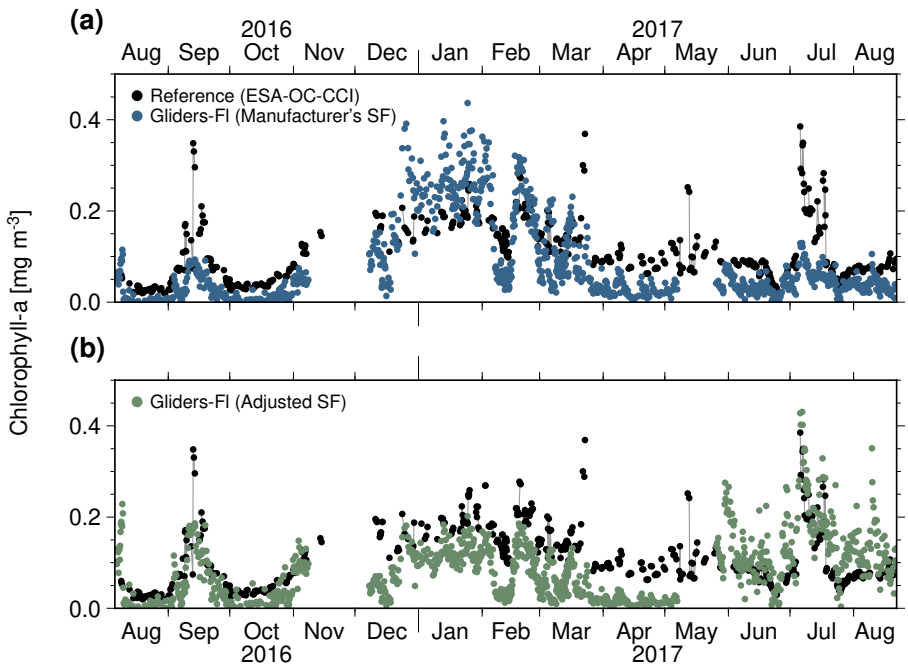

Figure 3. Comparisons of chlorophyll-a concentration estimated from satellite sensors and from glider's fluorescence calibrated using manufacturer's scale factor (a) and adjusted scale factors (b).

Satellite chlorophyll-a concentration is underestimated most of the year and overestimated in early winter from December 2016 to January 2017 with the manufacturer scale factor. By contrast, adjusted scale factors reduce the underestimation of chlorophyll-a concentration. It means that during some periods, the adjusted scale factor can improve the estimation of chlorophyll-a relative to the values obtained with the manufacturer's scale factor (Figure 3a). The bias can be computed (in the logarithm scale) following Seegers et al. (2018):

$$bias = 10^{\sum log(CHL_{gld} - CHL_{sat})}, \tag{3}$$

where CHL_{gld} is the chlorophyll-a estimated from glider fluorescence by using either the manufacturer or adjusted scale factors, and CHL_{sat} is the satellite chlorophyll-a concentration. Table 3 shows a large bias using both, the manufacturer's and adjusted scale factor. The manufacturer scale factor provides less biased chlorophyll-a concentration related to the adjusted scale factor in missions 0004 and 0005, whereas the adjusted scale factor reduces the bias during missions 0003 and 0006 (Table 3). However, none of the scale factors is consistently less biased than the other in all situations. In this work, the manufacturer scale factor is used to compute chlorophyll-a concentration from glider observations.

3.2 Physical and bio-optical variability inside the LCE Poseidon

Young Poseidon swirl speed was about $U = 70\,\mathrm{cm\,s^{-1}}$ in average, but then it decayed rapidly west of $-92\,\mathrm{W}$ to $30\,\mathrm{cm\,s^{-1}}$ (Figure 4a). LCE Poseidon moved hundreds of kilometers westwards at an averaged translation speed of c $\sim 4\,\mathrm{cm\,s^{-1}}$ (Figure 4b),

Table 3. The bias (see equation 3.1) of the chlorophyll-a concentration obtained with the manufacturer's and adjusted scale factors relative to the satellite-derived chlorophyll-a. Underestimation (overestimation) occurs for biases smaller (larger) than unity.

Mission	Bias (Manufacturer's SF)	Bias (Adjusted SF)
0003	0.35 (65 %)	0.70 (30 %)
0004	0.92 (8 %)	0.43 (57 %)
0005	0.52 (48 %)	0.30 (70 %)
0006	0.42 (58 %)	1.41 (41 %)

leading to a non-linearity parameter U/c always larger than unity (Figure 4c), suggesting that fluid is trapped during Poseidon's entire life (Flierl, 1981).

The potential density anomaly (σ_θ) and squared Brunt–Väisälä frequency ($N^2 = (-g/\sigma_0)\cdot\partial\sigma_\theta/\partial z$) are used to describe the seasonal cycle of the thermohaline vertical structure of LCE Poseidon (Figure 5a-b). The σ_θ and MLD have marked seasonal cycles with lighter upper waters and a shallower mixed layer in the summer, and heavier waters and deeper mixed layers during winter. In addition, summer seasonal pycnocline (at $\sim 30-50$ m) separates the mixed-layer from the pycnostad of the eddy located between 50 and 200 m depth (Figure 5b; mission 0003). The MLD increases during October 2016 (end of mission 0003) and by December reaches up to 150 m depth in agreement with the MLD climatology of Portela et al. (2018). The upper layer re-stratifies again in June 2017, forming a shallow 30 m mixed layer, and completing a full seasonal cycle.

The N^2 is large at the seasonal and main pycnocline ($> 1\times10^{-2}\,\mathrm{s}^{-2}$; Figure 5b). The main pycnocline of Poseidon holds the entire year at approximately 200 m depth, progressively weakening during eddy's translation westwards (Figure 5b). Contrary, winter convection due to the passage of cold fronts (Pérez et al., 2022; Zavala-Hidalgo et al., 2014) erodes completely the seasonal pycnocline, by mixing pycnostad and upper waters. Note that MLD and the depth of the $25.5\,\mathrm{kg\,m^{-3}}$ isopycnal (a proxy of the top of the nitracline) are only a few tens of meters apart during winter, and the alternative proxy of the nitracline (nitracline-VA22) overlap (Figure 5b), indicating that entrainment of nutrients could be possible.

The depth of the isopycnal of $25.5\,\mathrm{kg\,m^{-3}}$ is related to the spatial structure and dynamical stage of the eddy. In mission 0003, the glider sampled a young Poseidon located east -92 W (Figure 1a) with the isopycnal of $25.5\,\mathrm{kg\,m^{-3}}$ reaching up to 250 m depth in the center and ranging between $150-160$ m depth at the eddy edge (Figure 5c). Since December 2016 (beginning of mission 0004), the depth of the isopycnal of $25.5\,\mathrm{kg\,m^{-3}}$ continuously decreases (Figure 5c) due to Poseidon's lost of heat and salt (Meunier et al., 2020).

Poseidon's decay, west of -92 W (Figure 4a) leads to upwelling of isopycnals. This process is through the eddy pumping, that is, $\partial\sigma_\theta/\partial t > 0$ (Klein & Lapeyre, 2009). During December 2016 and January 2017 (mission 0004), the $25.5\,\mathrm{kg\,m^{-3}}$ isopycnal was at ~ 170 m depth and the normalized radius ranged between $R \in [0.25-0.75]$ (Figure 5c) suggesting that the glider drifted anticyclonically with the depth-averaged currents around the central region of Poseidon. Notice that near the peripheries of the eddy ($R \geq 1$), horizontal advection and sub-mesoscale ageostrophic processes dominate the variability of biogeochemical variables (Mahadevan et al., 2008; Chelton, Gaube, et al., 2011). However, these processes are out of the scope of this work because the analyses focused on the bio-optical properties near the eddy core ($R < 0.55$).

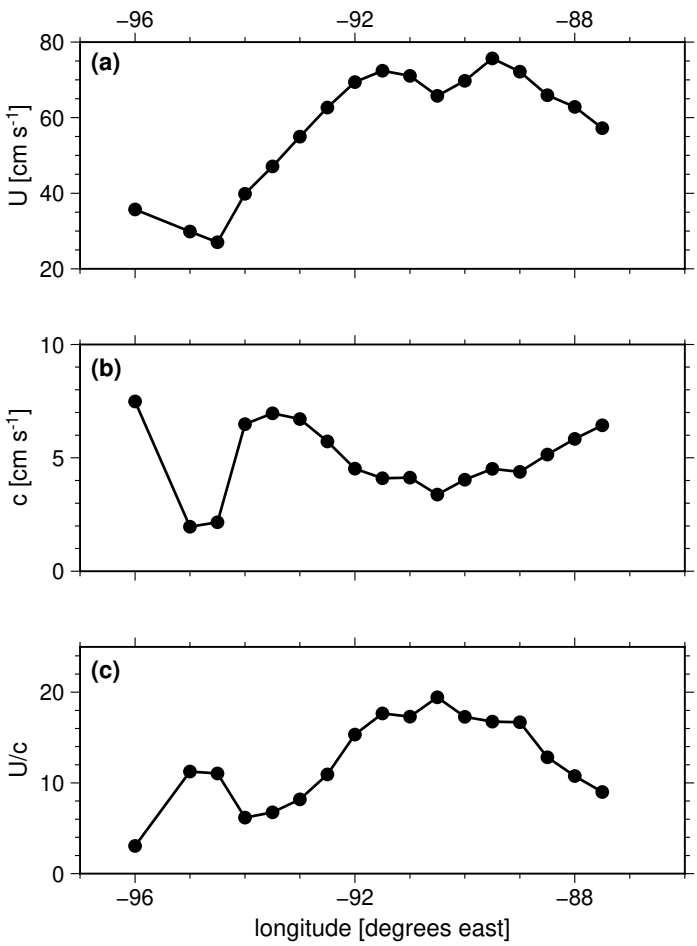

Figure 4. LCE Poseidon dynamical properties along its trajectory across the GoM: (a) swirl speed (U), (b) translation speed (c), and (c) non-linearity parameter (Flierl (1981); U/c).

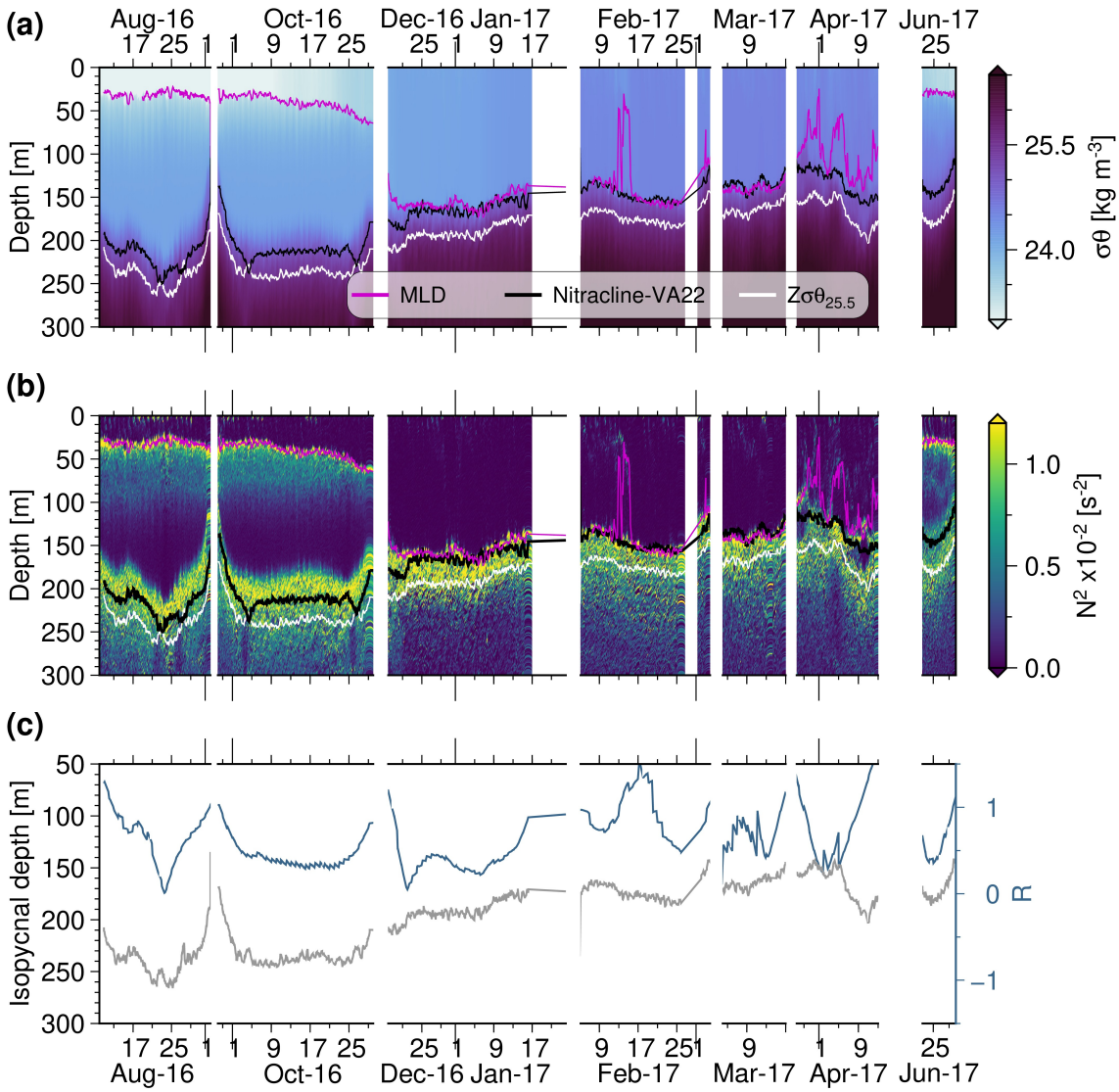

Figure 5. Distribution of (a) potential density anomaly referred at the surface (σ_0) and (b) squared Brunt–Väisälä frequency (N^2) as a function of depth. In (a-b), the magenta and white lines represent the MLD and the $25.5\,\mathrm{kg\,m^{-3}}$ isopycnal depth respectively. The black line is the alternative proxy of the top of the nitracline ($[N + N] > 0.5\,\mu\mathrm{mol\,kg^{-1}}$) based on empirical relations of hydrographic variables and nutrients (Velásquez-Aristizábal et al. (2022); nitracline-VA22). Panel (c) shows the depth of the $25.5\,\mathrm{kg\,m^{-3}}$ isopycnal (black line) and normalized glider location (R; blue line).

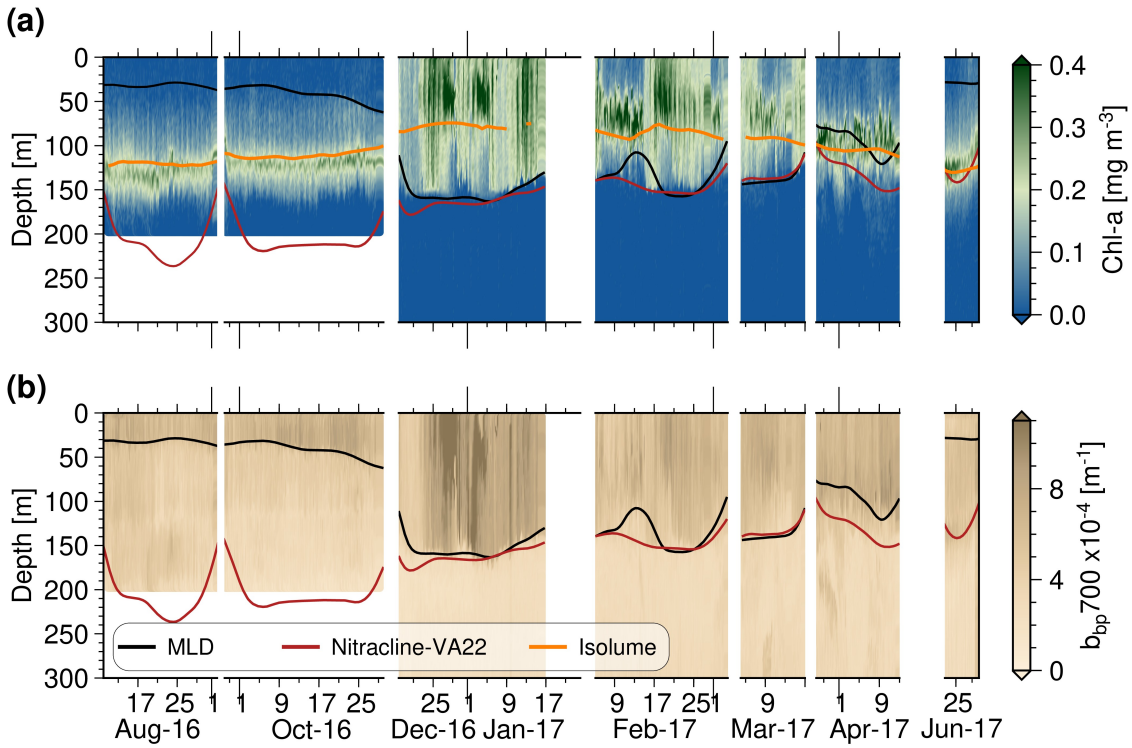

Figure 6. Vertical distribution of bio-optical properties collected inside the LCE Poseidon along a seasonal cycle as a function of depth. (a) Chlorophyll-a concentration by using the manufacturer scale factor and (b) the particle backscattering coefficient at 700 nm ($b_{bp}700$). The lines in b and c are the smoothed time series of the MLD (black), and the 0.08 isolume (orange). The red line corresponds to the top of the nutricline based on the Velásquez-Aristizábal et al. (2022) method (nitracline-VA22). The smoothed time series were obtained after using a 1D-LOESS to attenuate variability with periods below 3 days.

Contrasting conditions between summer and winter in terms of stratification affected the bio-optical variability across LCE Poseidon (Figure 6). During summer and early fall, the chlorophyll-a was extremely low within the MLD, with a DCM located at 130 m depth; 100 m shallower than the nitracline (Figure 6a). Between December 2016 and March 2017, the chlorophyll-a was mostly distributed through the whole mixed layer, with episodic sub-surface enhancements (Figure 6a). Since April 2017, the DCM becomes a stable structure when the upper ocean stratifies and the MLD shoals. The location of the DCM during the whole period approximately follows the ~ 0.08 isolume (Figure 6a), indicating that photoacclimation is an important process in regulating the vertical distribution of chlorophyll-a (Letelier et al., 2004; Mignot et al., 2014).

The $b_{bp}700$ vertical distribution (Figure 6b) is similar to chlorophyll-a concentration except during summer and spring. In summer of 2016, maximum values of $b_{bp}700$ were found in the mixed-layer (< 50 m) while the maximum chlorophyll-a was located in the DCM (Figure 6a and b). On December 25, 2016, $b_{bp}700$ intensified abruptly inside the core of Poseidon (Figure 6b) and remained elevated until January 17, 2017, with similar subsurface enhancements than chlorophyll-a concentration (Figure 6a and b). $b_{bp}700$ progressively decreases inside Poseidon towards summer of 2017. The enhancement of $b_{bp}700$ observed during winter is unlikely to be driven by horizontal or vertical advection, because the $b_{bp}700$ signal below the MLD was low, and the glider was near the cen-

ter between December and January. Thus, data suggest that appropriate environmental conditions stimulated phytoplankton production within the winter MLD of the LCE Poseidon.

3.3 Seasonal cycle of integrated chlorophyll-a and $b_{bp}700$ in the upper 200 m

Figure 7 shows the time evolution of chlorophyll-a concentration and $b_{bp}700$ integrated from surface to 200 m depth. The vertical integration of bio-optical properties has a double purpose: (i) removing the vertical variability and (ii) assessing the occurrence and reliability of a seasonal cycle of phytoplankton biomass not only at the sea surface but also within the euphotic layer. To analyze the seasonal cycle, the trend in bio-optical signals was removed first. Then, ordinary least-squares were used to fit the seasonal cycle, defined by the contribution of the mean and the annual and semi-annual harmonics:

$$F_{seas}(t) = F_0 + A_a \cdot cos(\omega t - \phi_a) + A_s \cdot cos(2\omega t - \phi_s) \tag{4}$$

where F_0 represents the mean. A_a and A_s are the amplitude of the annual and semi-annual harmonics. ϕ_a and ϕ_s are the phase of the annual and semi-annual harmonics, and ω is Earth's angular frequency ($2\pi f$; $f = 1/365.25\,\text{days}^{-1}$).

The analysis of the integrated variables showed that the seasonal cycle of chlorophyll-a observed at the surface (Figure 3) even holds when *in situ* chlorophyll-a concentration is vertically integrated (see for instance Pasqueron et al. (2017)). In addition, the seasonal cycles of both integrated chlorophyll-a concentration and $b_{bp}700$ (thick blue lines in Figure 7) were in phase, with maxima values (minima) in winter (summer). The seasonal cycle accounts for a significant fraction of the total variance in both bio-optical variables (Figure 7a and b).

The remaining fraction of the variance seems to be associated with high-frequency processes mostly noticed on the chlorophyll-a during winter, from December 2016 to January 2017 (Figure 6a and 7a). They are noticeable in the integrated variables as considerable departures from the seasonal cycle (see grey dots in Figure 7a). Thus, processes at short temporal scales could be important for modulating the distribution of bio-optical properties inside the eddy. By contrast, during spring and summer, the variability of chlorophyll-a is notably reduced in agreement with quiescent environmental conditions.

4 Discussion

The dataset used here has already contributed to improving understanding of the vertical distribution of physical properties (Meunier, Pallás-Sanz, et al., 2018; Portela et al., 2018), water mass transformation (Sosa-Gutiérrez et al., 2020), and physical submesoscale processes inside the LCE Poseidon (Meunier, Tenreiro, et al., 2018; Meunier et al., 2019). This is possible because underwater gliders can measure the properties of slow-moving mesoscale structures with high temporal and spatial resolution. Here, four glider missions were used to shed some light on the dynamics of phytoplankton in large LCEs.

During autumn and winter, the passage of several cold fronts increased the turbulent heat fluxes (latent and sensible) in the upper MLD of Poseidon, promoting gravitational instabilities inside the eddy core (Pérez et al., 2022). Thermal convection associated with (cold) northerly winds rapidly deepens the MLD (Pérez et al., 2022; Zavala-Hidalgo et al., 2014), which in the LCE Poseidon reaches up to 170 m depth, very close to the nitracline (Figure 5). A deeper MLD, closer to the nitracline, can increase the injection of nutrients into the euphotic zone through vertical diffusion, as it occurs with

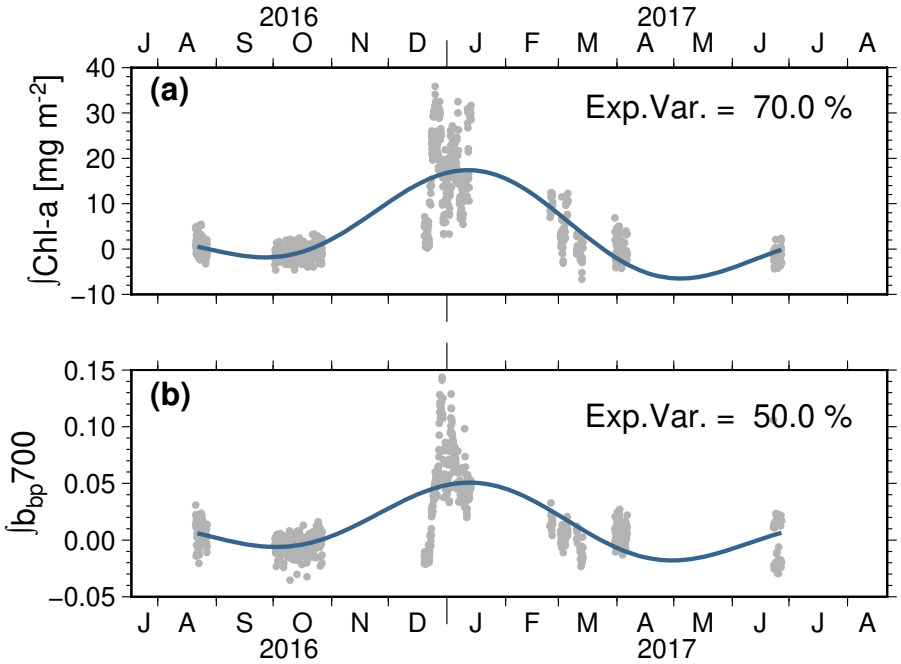

Figure 7. Seasonal variability of vertically integrated (0 − 200 m) chlorophyll-a (Chl-a) concentration and particle backscattering coefficient at 700 nm ($b_{bp}700$) inside the core of Poseidon: only are plotted measurements with $R < 0.55$. The blue line represents the fitted seasonal cycle, and the amount of explained variance (Exp.Var.) by the seasonal cycle is shown. The chlorophyll-a concentration from *in vivo* fluorescence was obtained with the manufacturer's scale factor.

salt (Sosa-Gutiérrez et al., 2020). The strong mixing during the passage of cold fronts separates the physical response of the GoM between stratified and mixed conditions with consequences for the local phytoplankton populations.

A stratified water column led to the development of a well-defined DCM, which is maintained until winter mixing tends to homogenize the bio-optical properties in the upper 200 m (Figure 6). The presence of DCM and the lack of sub-surface maximum in the $b_{bp}700$ signal during summer and spring (Figure 6a and b), suggests that the DCM arises from photoacclimation in response to the low-light levels at the bottom of the productive layer. A result that agrees with Linacre et al. (2019), which found a higher biomass of autotrophic organisms at the surface during summer.

A photoaclimation-driven DCM in the GoM has been reported since the work of Steele (1964). Steele's ideas were indeed included in the framework developed by Cullen (2015) to explain the mechanisms generating DCMs under different trophic regimes, pointing out that DCMs produced by photoacclimation are characteristic of oligotrophic environments, as has already been observed in several studies (Letelier et al., 2004; Barbieux et al., 2018; Mignot et al., 2014) and more recently supported in the case of the GoM deep waters (Linacre et al., 2019).

Changes observed in the relation between chlorophyll-a concentration and fluorescence are remarkable (Figure 2 and Table 2). The highest uncertainties in the model coefficients occur during winter (Table 2). Also, during the winter mission 0004, the highest dispersion from the fitted line was possibly associated with the sampling pattern. After reaching the eddy center, the compass failed. Then, the glider started to drift with the depth-averaged velocity, eventually close to the contour of maximum velocity. The sampling pattern of the glider during mission 0004 convolves the spatial and temporal variability as the glider moves anticyclonically within the LCE.

Variations in the physical and chemical conditions across the eddy can impact the taxonomic composition or nutritional status of phytoplankton cells. As a consequence, fluorescence emission can vary spatially inside the LCE. Hence, when analyzed together, the measurements near the center and towards the peripheries, the combination of factors increase the bio-optical variability, complicating the use of a single linear relation to derive the adjusted scale factor. In other words, the different factors affecting fluorescence emission act as confounding factors in the regression analysis, reducing the explained variance by the linear model ($r^2 = 0.46$ in Table 2).

On the other hand, the highest slopes were obtained during missions 0004 and 0005 (winter), whereas missions 0003 and 0006 (summer) showed the lowest slopes(Table 1). The variability in the magnitude of the slopes was not related to specific sensors. Gliders in missions 0004 and 0005 used different fluorometers (SNs: 1374 and 1375), yet the slopes were comparable (Table 1). Moreover, the same sensor (SN: 1374) was used during missions 0003 and 0006, but slopes differed by one order of magnitude between them (Table 1). Thus, the observed changes might be associated with seasonally dependent biogeochemical processes.

A shift in the taxonomic composition of the phytoplankton populations can cause changes in the slopes of the linear regressions because it is a factor of primary importance in the relationship between fluorescence and chlorophyll-a (Proctor & Roesler, 2010; C. S. Roesler & Barnard, 2013; C. Roesler et al., 2017). The seasonal succession of phytoplankton groups between summer and winter can occur inside the LCEs and likely through the GoM, and it will depend on at least two factors: (i) the winter mixing that redistributes phytoplankton populations and (ii) the seasonal changes of the environmental conditions (i.e. temperature, salinity, nutrient concentration, and irradiance). The redistribution of phytoplankton populations during winter was already considered in previous studies (Pasqueron et al., 2017; Linacre et al., 2015), while numerical models sug-

gest changes in phytoplankton community composition (Damien et al., 2021; Gomez et al., 2018). However, to our knowledge, it is the first time that observations support a shift in the taxonomic composition of phytoplankton in the GoM based on *in situ* optical data.

During summer, bio-optical data indicate the presence of two types of populations: (i) phytoplankton associated with the DCM with high chlorophyll-a and low $b_{bp}700$, adapted to environments with low light availability and temperature at the base of the productive layer; and (ii) phytoplankton living near the surface under higher irradiance and temperature, characterized by low chlorophyll-a and high $b_{bp}700$ (Figure 6a and b).

The occurrence of different groups along a stratified water column agrees with the results of the cytometric and genetic analysis presented by Linacre et al. (2019). They found high-light adapted ecotypes of *Prochlorococcus* at the surface and low-light adapted cells at the base of the euphotic layer. During winter, these populations are mixed, but lower irradiance and lower temperatures, driven by the upper ocean seasonal cycle can favor the phytoplankton of the lower euphotic zone already adapted to low light and lower temperatures. Here, it is important to note that fluorescence emission per unit of chlorophyll-a increases as irradiance decreases in *Prochlorococcus*, and both chlorophyll-a concentration and fluorescence emission, tend to be higher in low-light adapted ecotypes (Moore et al., 1995). A succession of phytoplankton populations is thus possible at the ecotype level of differentiation of the picoplanktonic *Prochlorococcus*.

Succession between different size groups (pico to nanophytoplankton) is also possible, and actually, it is a result of numerical simulations of the GoM's ecosystem (Damien et al., 2018; Gomez et al., 2018; Damien et al., 2021). It is an accepted paradigm in phytoplankton ecology, associated with changes in turbulence and nutrient availability (Cullen et al., 2002; Margalef, 1978). Some opportunistic species of nanoplankton like *Emiliania huxleyi*, could be favored during the winter conditions if the amounts of new nutrients entrained in the euphotic layer are significant.

A winter increase of the nutrient concentration inside LCEs can be driven primarily by vertical diffusion when the MLD reaches or extends below the nitracline (Damien et al., 2021). Although the MLD does not reach the $25.5\,\mathrm{kg\,m^{-3}}$ isopyncal (proxy of the top of the nitracline; Figure 6), the entrainment of nutrients cannot be ruled out. Direct observations of [N+N] profiles, including stations inside Poseidon during its early stages, show that nitracline is shallower than the $25.5\,\mathrm{kg\,m^{-3}}$ isopyncal (Lee-Sánchez et al., 2022). Thus, it is concluded that the [N+N] depletion depth was shallower than the MLD during winter inside the LCE Poseidon as indicated by the alternative proxy of the nitracline (Figure 5a and b).

Hence, Pasqueron's criteria, used here to define the [N+N] depletion depth, flaws inside the large LCE Poseidon. However, alternative methods are also error-prone when large LCEs are analyzed. Indeed, (Velásquez-Aristizábal et al., 2022) showed that was difficult to predict the vertical distribution of nutrients within the LCE Poseidon based on hydrographic proxies, given its anomalously low concentration of nutrients in upper layers. It means that nitracline-VA22 used here can be an underestimation.

Another result that supports the increase in nutrient concentration in the euphotic zone, is indeed based on the seasonal cycle of the chlorophyll-a and $b_{bp}700$ integrated in the upper 200 m. Whereas the chlorophyll-a seasonal cycle can be questioned due to the changes in the relation between chlorophyll-a and fluorescence (Figure 2), the $b_{bp}700$ is a proxy of phytoplankton carbon (Graff et al., 2015) that increases during winter, in phase with the chlorophyll-a concentration (Figure 7). This concomitant change of bio-optical variables supports the idea of a winter enhancement of the phytoplankton biomass, which is difficult to explain without invoking nutrient injection. Especially inside the core of LCEs which remained isolated from surrounding waters.

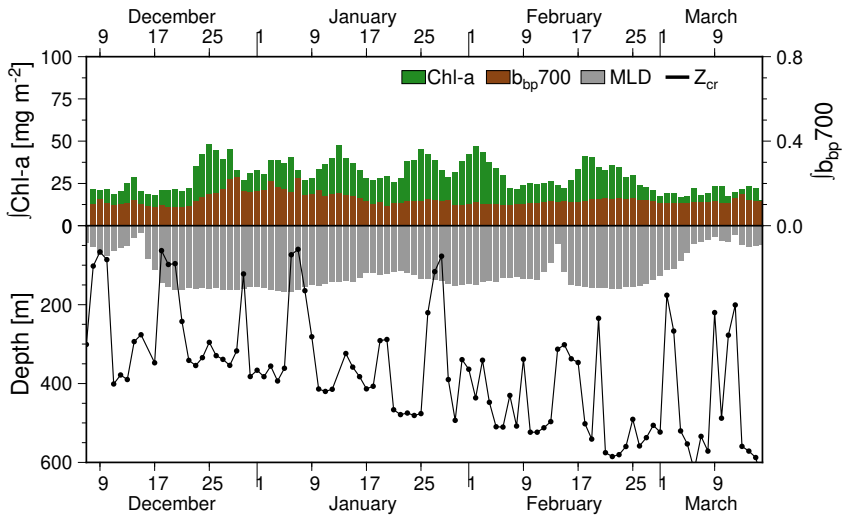

Figure 8. Winter bio-optical variability and its relation to the changes of the MLD and Sverdrup's critical depth. Only winter data was used because is the season when MLD reaches its maximum depth, whereas irradiance decreases by the solar cycle and the shorter day length. In the upper panel, green bars represent the integrated chlorophyll-a in the upper 200 m, while the integrated $b_{bp}700$ (proxy of phytoplankton carbon) are to the brown bars. Data were daily averaged, and the the MLD (gray bars) and Sverdrup's critical depth (black-dotted line) are depicted. According to Sverdrup (1953), low irradiance can inhibit a net phytoplankton growth when MLD exceeds the critical depth.

Alternative explanations for the increase in the $b_{bp}700$ during winter can be related to changes in phytoplankton composition, as in the case of the chlorophyll-a fluorescence. However, what process could promote changes in phytoplankton composition? Again, the answer can be associated with the increase in the nutrient concentration by vertical diffusion, which arises as a plausible and parsimonious process to explain the observed patterns in the bio-optical variables. Nonetheless, the increase in phytoplankton biomass during winter can be modified by changes in the loss-term (i.e. grazing, viral infection, sinking) of phytoplankton cells, as suggested in other studies (Behrenfeld, 2010; Behrenfeld & Boss, 2014).

A comparison between the MLD and Sverdrup's critical depth is used to assess the light effects on phytoplankton growth. The analyses showed that inhibition due to low-light conditions during winter does not occur for extended periods. MLD only exceeds the critical depth for short time lapses of 1-3 days (Figure 8). As the computation of the critical depth relied on constant $Kd(PAR)$ and Ed_c, the variability is produced by changes in the irradiance at the sea surface, probably by the cloud coverage associated with the passage of cold atmospheric fronts. In addition, the DCM followed approximately the depth of the 0.08 isolume, indicating that phytoplankton is photoacclimated, and presumably cannot fix carbon through photosynthesis below this threshold on irradiance, in agreement with experimental works (Moore et al., 1995).

Finally, high-frequency variability in the bio-optical properties is noticeable, especially on chlorophyll-a estimated from *in vivo* fluorescence, which is a variable that responds rapidly to the changes in irradiance (Lewis et al., 1984). Patches of enhanced subsurface chlorophyll-a concentration occur inside the mixed layer at 5-day periods (Figure 6b). This variability is related to the passage of cold fronts, characterized by bursts of high speed lasting a few days and influencing the upper layer in the GoM, by turbu-

lent heat exchange and mechanical input of energy during autumn and winter seasons (Pérez et al., 2022; Zavala-Hidalgo et al., 2014). These processes occurring at 5-day periods can not be resolved by profiling the water column every 10-14 days with Argo floats, highlighting the capabilities of gliders to capture the ocean's short-term variability, which can impact phytoplankton dynamics (Platt et al., 1989). Thus, glider data can complement observations made with other valuable platforms monitoring the ocean at other scales such as the Argo floats and research vessels.

High-frequency variability of bio-optical properties is out of the scope of this paper. Future work will focus on assessing the effect of atmospheric forcing (wind and air temperature) on the occurrence and shutdown of strong convective turbulence, which can modulate phytoplankton dynamics (Lewis et al., 1984; Taylor & Ferrari, 2011). In addition, the role of Ekman pumping could be important especially when the MLD remains close to the top of the nitracline as occurred in the LCE Poseidon.

5 Conclusions

Analyses of physical and bio-optical measurements collected by underwater gliders showed concomitant seasonal variability between vertically integrated chlorophyll-a, and particle backscattering coefficient with maxima during winter. The relation between chlorophyll-a concentration and fluorescence was complex during winter, and especially during mission 0004. Seasonal varying slopes obtained from the linear regressions between chlorophyll-a and fluorescence could be related to changes in phytoplankton composition, as a response to the changes in temperature, nutrient concentration, and irradiance. Indeed, an enhancement in the nutrient concentration in the euphotic zone by vertical diffusion increased the phytoplankton biomass inside Poseidon LCE, which is supported by the increase in $b_{bp}700$. Comparison between the MLD and the Svedrup's critical depth suggests that low light during winter conditions is not a limiting factor for most of the year but, it can occur during short lapses of time of 1-3 days given the cloudy atmospheric surges. The present work is in good agreement with previous findings based on numerical simulations, but new questions arise. The importance of top-down processes in the regulation of phytoplankton standing stocks was not solved, and its assessment continues to be a question mark in the ecosystem dynamics of the GoM during winter.

6 Open Research

The data used in this work can be downloaded on the group website (`https://gliders.cicese.mx/`), for the review process, and access can be granted by request to the corresponding author and lead of the project EPS.

Acknowledgments

This work was supported by the project *"Florecimientos Algales en un Remolino de la Corriente de Lazo"* from *Consejo Nacional de Humanidades, Ciencias y Tecnologías de México (CONAHCyT)*, and from the program *Hidrocarburos-SENER-CONACyT Consorcio de Investigaciones el Golfo de México* under the project *Implementación de redes de observaciones oceanográficas (físicas, geoquímicas, ecológicas) para la generación de escenarios ante posibles contingencias relacionadas a la exploración y producción de hidrocarburos en aguas profundas del Golfo de México(CIGoM)*. Both projects are lead by EPS and MT. AM was supported by CONAHCyT with a posdoctoral fellowship associated to the CVU:516117. We acknowledged the contribution of all the staff of Grupo de Monitoreo Oceanográfico con Gliders at CICESE, specially to Simo Cusí and Adrián Villicaña for piloting underwater gliders, and to Johanna Saavedra for data management of the glider's data. We acknowledge the effort of international agencies which give public access to satellite data used in this study. We are grateful to the European Space Agency

for allowing access to the version 5 of the ESA-CCI OC product. We are also grateful to the National Aeronautics and Space Administration that give public access to the EPICS/DISCOVR irradiance data. During early versions comments made by Dr. Xiomara Márquez-Artavia from Universidad Nacional de Costa Rica, helped to improve the work.

References

Bailey, S. W., & Werdell, P. J. (2006, 5). A multi-sensor approach for the on-orbit validation of ocean color satellite data products. *Remote Sensing of Environment*, *102*, 12-23. doi: 10.1016/j.rse.2006.01.015

Banse, K. (2004). Should we continue to use the 1compensation depth of phytoplankton for another 70 years? *Limnology and Oceanography Bulletin*, *13*, 49-52. Retrieved from `http://doi.wiley.com/10.1002/lob.200413349` doi: 10.1002/lob.200413349

Barbieux, M., Uitz, J., Bricaud, A., Organelli, E., Poteau, A., Schmechtig, C., ... Claustre, H. (2018). Assessing the variability in the relationship between the particulate backscattering coefficient and the chlorophyll a concentration from a global biogeochemical-argo database. *Journal of Geophysical Research: Oceans*, *123*, 1229-1250. doi: 10.1002/2017JC013030

Barceló-Llull, B., Pallàs-Sanz, E., Sangrà, P., Martínez-Marrero, A., Estrada-Allis, S. N., & Arístegui, J. (2017, 5). Ageostrophic secondary circulation in a subtropical intrathermocline eddy. *Journal of Physical Oceanography*, *47*, 1107-1123. doi: 10.1175/JPO-D-16-0235.1

Behrenfeld, M. J. (2010). Abandoning sverdrup's critical depth hypothesis on phytoplankton blooms. *Ecology*, *91*, 977-989. doi: 10.1890/09-1207.1

Behrenfeld, M. J., & Boss, E. S. (2014). Resurrecting the ecological underpinnings of ocean plankton blooms. *Annual Review of Marine Science*, *6*, 167-194. doi: 10.1146/annurev-marine-052913-021325

Biller, S. J., Berube, P. M., Lindell, D., & Chisholm, S. W. (2014). Prochlorococcus: the structure and function of collective diversity. *Nature Reviews Microbiology*, *13*, 13-27. Retrieved from `http://www.nature.com/doifinder/10.1038/nrmicro3378%5Cnhttp://dx.doi.org/10.1038/nrmicro3378` doi: 10.1038/nrmicro3378

Boss, E., Swift, D., Taylor, L., Brickley, P., Zaneveld, R., Riser, S., ... Strutton, P. G. (2008). Observations of pigment and particle distributions in the western north atlantic from an autonomous float and ocean color satellite. *Limnology and Oceanography*, *53*, 2112-2122. doi: 10.4319/lo.2008.53.5_part_2.2112

Briggs, N., Perry, M. J., Cetinić, I., Lee, C., D'Asaro, E., Gray, A. M., & Rehm, E. (2011). High-resolution observations of aggregate flux during a sub-polar north atlantic spring bloom. *Deep-Sea Research Part I: Oceanographic Research Papers*, *58*, 1031-1039. doi: 10.1016/j.dsr.2011.07.007

Chelton, D. B., Gaube, P., Schlax, M. G., Early, J. J., & Samelson, R. M. (2011, 10). The influence of nonlinear mesoscale eddies on near-surface oceanic chlorophyll. *Science*, *334*, 328-332. doi: 10.1126/science.1208897

Chelton, D. B., Schlax, M. G., & Samelson, R. M. (2011, 10). Global observations of nonlinear mesoscale eddies. *Progress in Oceanography*, *91*, 167-216. doi: 10.1016/j.pocean.2011.01.002

Chen, K. E., Gaube, P., & Pallàs-Sanz, E. (2020). On the vertical velocity and nutrient delivery in warm core rings. *Journal of Physical Oceanography*, *50*, 1557-1582. doi: 10.1175/JPO-D-19-0239.1

Concha, J. A., Bracaglia, M., & Brando, V. E. (2021, 6). Assessing the influence of different validation protocols on ocean colour match-up analyses. *Remote Sensing of Environment*, *259*. doi: 10.1016/j.rse.2021.112415

Cullen, J. J. (2015). Subsurface chlorophyll maximum layers: enduring enigma or mystery solved? *Annual review of marine science*, *7*, 207-39. Re-

trieved from http://www.ncbi.nlm.nih.gov/pubmed/25251268 doi: 10.1146/annurev-marine-010213-135111

Cullen, J. J., Franks, P. J. S., Karl, D. M., & Longhurst, A. (2002). Physical influences on marine ecosystem dynamics. In A. R. Robinson, J. J. McCarthy, & B. J. Rothschild (Eds.), (Vol. 12, p. 297-336). John Wiley and Sons.

Damien, P., de Fommervault, O. P., Sheinbaum, J., Jouanno, J., Camacho-Ibar, V. F., & Duteil, O. (2018, 4). Partitioning of the open waters of the gulf of mexico based on the seasonal and interannual variability of chlorophyll concentration. *Journal of Geophysical Research: Oceans*, *123*, 2592-2614. doi: 10.1002/2017JC013456

Damien, P., Sheinbaum, J., Fommervault, O. P. D., Jouanno, J., Linacre, L., & Duteil, O. (2021, 7). Do loop current eddies stimulate productivity in the gulf of mexico? *Biogeosciences*, *18*, 4281-4303. doi: 10.5194/bg-18-4281-2021

Ekman, V. W. (1905). On the influence of the earth's rotation on ocean-currents. *Arkiv För Matematik, Astronomi Och Fysik*, *2*, 1-53.

Estrada-Allis, S. N., Barceló-Llull, B., Pallàs-Sanz, E., Rodríguez-Santana, A., Souza, J. M., Mason, E., ... Sangrà, P. (2019). Vertical velocity dynamics and mixing in an anticyclone near the canary islands. *Journal of Physical Oceanography*, *49*, 431-451. doi: 10.1175/JPO-D-17-0156.1

Falkowski, P. G., Ziemann, D., Kolber, Z., & Bienfang, P. K. (1991). Role of eddy pumping in enhancing primary production in the ocean. *Nature*, *352*, 55-58.

Flierl, G. R. (1981). Particle motions in large-amplitude wave fields. *Geophysical & Astrophysical Fluid Dynamics*, *18*, 39-74. doi: 10.1080/03091928108208773

Flierl, G. R., & Mied, R. P. (1985, 9). Frictionally induced circulations and spin down of a warm-core ring. *Journal of Geophysical Research*, *90*, 8917. doi: 10.1029/jc090ic05p08917

Fox, J. (2016). *Applied regression analysis and generalized linear models* (Third ed.). SAGE.

Franks, P. J. (2015, 5). Has sverdrup's critical depth hypothesis been tested? mixed layers vs. turbulent layers. *ICES Journal of Marine Science*, *72*, 1897-1907. doi: 10.1093/icesjms/fsu175

Franks, P. J. S., Wroblewski, J. S., & Flierl, G. R. (1986). Prediction of phytoplankton growth in response to the frictional decay of a warm-core ring. *Journal of Geophysical Research*, *91*, 7603. doi: 10.1029/jc091ic06p07603

Frouin, R., Tan, J., Compiègne, M., Ramon, D., Sutton, M., Murakami, H., ... Vellucci, V. (2022, 4). The nasa epic/dscovr ocean par product. *Frontiers in Remote Sensing*, *3*, 1-17. doi: 10.3389/frsen.2022.833340

Frouin, R. J., Tan, J., Franz, B., Murakami, H., & Ramon, D. (2018, 10). Estimating photosynthetically available radiation at the ocean surface from epic/dscovr data. In (p. 5). SPIE-Intl Soc Optical Eng. doi: 10.1117/12.2501675

Gaube, P., Chelton, D. B., Strutton, P. G., & Behrenfeld, M. J. (2013). Satellite observations of chlorophyll, phytoplankton biomass, and ekman pumping in nonlinear mesoscale eddies. *Journal of Geophysical Research: Oceans*, *118*, 6349-6370. doi: 10.1002/2013JC009027

Gomez, F. A., Lee, S. K., Liu, Y., Hernandez, F. J., Muller-Karger, F. E., & Lamkin, J. T. (2018, 6). Seasonal patterns in phytoplankton biomass across the northern and deep gulf of mexico: A numerical model study. *Biogeosciences*, *15*, 3561-3576. doi: 10.5194/bg-15-3561-2018

Gordon, H. R., Clark, D. K., Brown, J. W., Brown, O. B., Evans, R. H., & Broenkow, W. W. (1983). Phytoplankton pigment concentrations in the middle atlantic bight: comparison of ship determinations and czcs estimates. *Applied Optics*, *22*, 20-36.

Graff, J. R., Westberry, T. K., Milligan, A. J., Brown, M. B., Dall'Olmo, G., van Dongen-Vogels, V., ... Behrenfeld, M. J. (2015, 8). Analytical phytoplankton

carbon measurements spanning diverse ecosystems. *Deep-Sea Research Part I: Oceanographic Research Papers*, *102*, 16-25. doi: 10.1016/j.dsr.2015.04.006

He, Q., Zhan, H., Shuai, Y., Cai, S., Li, Q. P., Huang, G., & Li, J. (2017, 6). Phytoplankton bloom triggered by an anticyclonic eddy: The combined effect of eddy-ekman pumping and winter mixing. *Journal of Geophysical Research: Oceans*, *122*, 4886-4901. doi: 10.1002/2017JC012763

Hoskins, B. J., Draghici, I., & Davies, H. C. (1978). A new look at the w-equation. *uarterly Journal of the Royal Meteorological Society*, *104*, 31-38.

Klein, P., & Lapeyre, G. (2009). The oceanic vertical pump induced by mesoscale and submesoscale turbulence. *Annual Review of Marine Science*, *1*, 351-375.

Lavigne, H., D'Ortenzio, F., Migon, C., Claustre, H., Testor, P., D'Alcalà, M. R., ... Prieur, L. (2013, 7). Enhancing the comprehension of mixed layer depth control on the mediterranean phytoplankton phenology. *Journal of Geophysical Research: Oceans*, *118*, 3416-3430. doi: 10.1002/jgrc.20251

Lee-Sánchez, E., Camacho-Ibar, V. F., Velásquez-Aristizábal, J. A., Valencia-Gasti, J. A., & Samperio-Ramos, G. (2022, 5). Impacts of mesoscale eddies on the nitrate distribution in the deep-water region of the gulf of mexico. *Journal of Marine Systems*, *229*. doi: 10.1016/j.jmarsys.2022.103721

Letelier, R. M., Karl, D. M., Abbott, M. R., & Bidigare, R. R. (2004). Light driven seasonal patterns of chlorophyll and nitrate in the lower euphotic zone of the north pacific subtropical gyre. *Limnology and Oceanography*, *49*, 508-519. doi: 10.4319/lo.2004.49.2.0508

Lewis, M. R., p W Horne, E., Cullen, J. J., Oakey, N. S., & Platt, T. (1984). Turbulent motions may control phytoplankton photosynthesis in the upper ocean. *Nature*, *311*, 49-50.

Linacre, L., Durazo, R., Camacho-Ibar, V. F., Selph, K. E., Lara-Lara, J. R., Mirabal-Gómez, U., ... Sidón-Ceseña, K. (2019, 11). Picoplankton carbon biomass assessments and distribution of prochlorococcus ecotypes linked to loop current eddies during summer in the southern gulf of mexico. *Journal of Geophysical Research: Oceans*, *124*, 8342-8359. doi: 10.1029/2019JC015103

Linacre, L., Lara-Lara, R., Camacho-Ibar, V., Herguera, J. C., Bazán-Guzmán, C., & Ferreira-Bartrina, V. (2015, 12). Distribution pattern of picoplankton carbon biomass linked to mesoscale dynamics in the southern gulf of mexico during winter conditions. *Deep-Sea Research Part I: Oceanographic Research Papers*, *106*, 55-67. doi: 10.1016/j.dsr.2015.09.009

Liu, H., Zhu, M., Guo, S., Zhao, X., & Sun, X. (2020, 5). Effects of an anticyclonic eddy on the distribution and community structure of zooplankton in the south china sea northern slope. *Journal of Marine Systems*, *205*. doi: 10.1016/j.jmarsys.2020.103311

Mahadevan, A., Thomas, L. N., & Tandon, A. (2008, 4). Comment on "eddy/wind interactions stimulate extraordinary mid-ocean plankton blooms". *Science*, *320*. doi: 10.1126/science.1152111

Mann, K. H., & Lazier, J. R. N. (2006). *Dynamics of marine ecosystems. biological-physical interactions in the oceans* (Third ed.).

Margalef, R. (1978). Life-forms of phytoplankton as survival alternatives in an unstable environment. *Oceanologica Acta*, *1*, 493-509.

Martin, A. P., & Richards, K. J. (2001). Mechanisms for vertical nutrient transport within a north atlantic mesoscale eddy. *Deep-Sea Research II*, *48*, 757-773.

McGillicuddy, D. J. (2016). Mechanisms of physical-biological-biogeochemical interaction at the oceanic mesoscale. *Annual Review of Marine Science*, *8*, 125-159. Retrieved from `http://www.annualreviews.org/doi/10.1146/annurev-marine-010814-015606` doi: 10.1146/annurev-marine-010814-015606

McGillicuddy, D. J., Anderson, L. A., Bates, N. R., Bibby, T., Buesseler, K. O., Carlson, C. A., ... Steinberg, D. K. (2007). Eddy/wind interactions stimulate extraordinary mid-ocean plankton blooms. *Science*, *316*, 1021-1026. Retrieved

from http://www.sciencemag.org/content/316/5827/1021.abstract doi: 10.1126/science.1136256

McGillicuddy, D. J., Robinson, A. R., Siegel, D. A., Jannasch, H. W., Johnson, R., Dickey, T. D., ... Knap, A. H. (1998). Mcgillicuddy-influence of mesoscale eddies on new production in the sargasso sea. *Nature*, *394*, 263-266.

McGillicuddy, D. J., & Robinson-F, A. R. (1997). Eddy-induced nutrient supply and new production in the sargasso sea. *Deep-Sea Research I*, *44*, 1427-1450.

Meunier, T., Pallás-Sanz, E., Tenreiro, M., Portela, E., Ochoa, J., Ruiz-Angulo, A., & Cusí, S. (2018, 9). The vertical structure of a loop current eddy. *Journal of Geophysical Research: Oceans*, *123*, 6070-6090. doi: 10.1029/2018JC013801

Meunier, T., Sanz, E. P., Tenreiro, M., Ochoa, J., Angulo, A. R., & Buckingham, C. (2019, 12). Observations of layering under a warm-core ring in the gulf of mexico. *Journal of Physical Oceanography*, *49*, 3145-3162. doi: 10.1175/JPO-D-18-0138.1

Meunier, T., Sheinbaum, J., Pallàs-Sanz, E., Tenreiro, M., Ochoa, J., Ruiz-Angulo, A., ... de Marez, C. (2020, 2). Heat content anomaly and decay of warm-core rings: the case of the gulf of mexico. *Geophysical Research Letters*, *47*. doi: 10.1029/2019GL085600

Meunier, T., Tenreiro, M., Pallàs-Sanz, E., Ochoa, J., Ruiz-Angulo, A., Portela, E., ... Carton, X. (2018, 8). Intrathermocline eddies embedded within an anticyclonic vortex ring. *Geophysical Research Letters*, *45*, 7624-7633. doi: 10.1029/2018GL077527

Mignot, A., Claustre, H., Uitz, J., Poteau, A., Ortenzio, F. D., & Xing, X. (2014). Understanding the seasonal dynamics and the deep chlorophyll maximum in oligotrophic environments: A bio-argo investigation. *Global Biogeochemical Cycles*, 856-876. doi: 10.1002/2013GB004781.Received

Mignot, A., Ferrari, R., & Claustre, H. (2018, 12). Floats with bio-optical sensors reveal what processes trigger the north atlantic bloom. *Nature Communications*, *9*. doi: 10.1038/s41467-017-02143-6

Moore, L. R., Goericke, R., & Chisholm, S. W. (1995). Comparative physiology of synechococcus and prochlorococcus: Influence of light and temperature on growth, pigments, fluorescence and absorptive properties. *Marine Ecology Progress Series*, *116*, 259-275. doi: 10.3354/meps116259

Morel, A., Huot, Y., Gentili, B., Werdell, P. J., Hooker, S. B., & Franz, B. A. (2007, 11). Examining the consistency of products derived from various ocean color sensors in open ocean (case 1) waters in the perspective of a multi-sensor approach. *Remote Sensing of Environment*, *111*, 69-88. doi: 10.1016/j.rse.2007.03.012

Muller-Karger, F. E., Smith, J. P., Werner, S., Chen, R., Roffer, M., Liu, Y., ... Enfield, D. B. (2015, 5). Natural variability of surface oceanographic conditions in the offshore gulf of mexico. *Progress in Oceanography*, *134*, 54-76. doi: 10.1016/j.pocean.2014.12.007

Muller-Karger, F. E., Walsh, J. J., Evans, R. H., & Meyers, M. B. (1991). On the seasonal phytoplankton concentration and sea surface temperature cycles of the gulf of mexico as determined by satellites. *Journal of Geophysical Research*, *96*, 12645-12665. Retrieved from https://digitalcommons.usf.edu/msc_facpub/78

Omand, M. M., & Mahadevan, A. (2015). The shape of the oceanic nitracline. *Biogeosciences*, *12*, 3273-3287. doi: 10.5194/bg-12-3273-2015

Pallàs-Sanz, E., & Álvaro Viúdez. (2005). Diagnosing mesoscale vertical motion from horizontal velocity and density data. *Journal of Physical Oceanography*, *35*, 1744-1762. doi: https://doi.org/10.1175/JPO2784.1.

Partensky, F., & Garczarek, L. (2010). Prochlorococcus : Advantages and limits of minimalism. *Annual Review of Marine Science*, *2*, 305-331. doi: 10.1146/annurev-marine-120308-081034

Partensky, F., Hess, W. R., & Vaulot, D. (1999). Prochlorococcus, a marine photosynthetic prokaryote of global significance. *Microbiology and molecular biology reviews*, *63*, 106-127. Retrieved from `http://www.ncbi.nlm.nih.gov/pubmed/10066832%0Ahttp://www.pubmedcentral.nih.gov/articlerender.fcgi?artid=PMC98958`

Pasqueron, D. F. O., Perez-Brunius, P., Damien, P., Camacho-Ibar, V. F., & Sheinbaum, J. (2017, 12). Temporal variability of chlorophyll distribution in the gulf of mexico: Bio-optical data from profiling floats. *Biogeosciences*, *14*, 5647-5662. doi: 10.5194/bg-14-5647-2017

Peterson, T. D., Crawford, D. W., & Harrison, P. J. (2011, 3). Evolution of the phytoplankton assemblage in a long-lived mesoscale eddy in the eastern gulf of alaska. *Marine Ecology Progress Series*, *424*, 53-73. doi: 10.3354/meps08943

Platt, T., Harrison, W. G., Lewis, M. R., Li, W. K. W., Sathyendranath, S., Smith, R. E., & Vezina, A. F. (1989). Biological production of the oceans: the case for a consensus. *Marine Ecology Progress Series*, *52*, 77-88. doi: 10.3354/meps052077

Portela, E., Tenreiro, M., Pallàs-Sanz, E., Meunier, T., Ruiz-Angulo, A., Sosa-Gutiérrez, R., & Cusí, S. (2018, 8). Hydrography of the central and western gulf of mexico. *Journal of Geophysical Research: Oceans*, *123*, 5134-5149. doi: 10.1029/2018JC013813

Proctor, C. W., & Roesler, C. S. (2010). New insights on obtaining phytoplankton concentration and composition from in situ multispectral chlorophyll fluorescence. *Limnology and Oceanography: Methods*, *8*, 695-708. doi: 10.4319/lom.2010.8.695

Pérez, J. G., Pallàs-Sanz, E., Tenreiro, M., Meunier, T., Jouanno, J., & Ruiz-Angulo, A. (2022, 4). Overturning instabilities across a warm core ring from glider observations. *Journal of Geophysical Research: Oceans*, *127*. doi: 10.1029/2021JC017527

Regaudie-De-Gioux, A., & Duarte, C. M. (2010). Compensation irradiance for planktonic community metabolism in the ocean. *Global Biogeochemical Cycles*, *24*. doi: 10.1029/2009GB003639

Roesler, C., Uitz, J., Claustre, H., Boss, E., Xing, X., Organelli, E., ... Barbieux, M. (2017). Recommendations for obtaining unbiased chlorophyll estimates from in situ chlorophyll fluorometers: A global analysis of wet labs eco sensors. *Limnology and Oceanography: Methods*, *15*, 572-585. doi: 10.1002/lom3.10185

Roesler, C. S., & Barnard, A. H. (2013). Optical proxy for phytoplankton biomass in the absence of photophysiology: Rethinking the absorption line height. *Methods in Oceanography*, *7*, 79-94. doi: 10.1016/j.mio.2013.12.003

Sathyendranath, S., Brewin, R. J., Brockmann, C., Brotas, V., Calton, B., Chuprin, A., ... Platt, T. (2019). An ocean-colour time series for use in climate studies: The experience of the ocean-colour climate change initiative (oc-cci). *Sensors (Switzerland)*, *19*. doi: 10.3390/s19194285

Schmechtig, C., Boss, E. S., Briggs, N. T., Claustre, H., Dall'Olmo, G., & Poteau, A. (2019). *Bgc argo quality control manual for particles backscattering* (Tech. Rep.). Argo Data Management Team. doi: 10.13155/60262

Schmechtig, C., Claustre, H., Poteau, A., & D'Ortenzio, F. (2018). *Bio-argo quality control manual for the chlorophyll-a concentration* (Tech. Rep.). Argo Data Management Team. doi: 10.13155/35385

Schmechtig, C., Poteau, A., Claustre, H., D'Ortenzio, F., Dall'Olmo, G., & Boss, E. S. (2018). *Processing bgc-argo particle backscattering at the dac level* (Tech. Rep.). doi: 10.13155/57195

Seegers, B. N., Stumpf, R. P., Schaeffer, B. A., Loftin, K. A., & Werdell, P. J. (2018). Performance metrics for the assessment of satellite data products: an ocean color case study. *Optics Express*, *26*, 7404. doi: 10.1364/oe.26.007404

Siegel, D. A., Doney, S. C., & Yoder, J. A. (2002, 4). The north atlantic spring phytoplankton bloom and sverdrup's critical depth hypothesis. *Science*, *296*, 730-733. doi: 10.1126/science.1069174

Siegel, D. A., Peterson, P., McGillicuddy, D. J., Maritorena, S., & Nelson, N. B. (2011, 7). Bio-optical footprints created by mesoscale eddies in the sargasso sea. *Geophysical Research Letters*, *38*. doi: 10.1029/2011GL047660

Sosa-Gutiérrez, R., Pallàs-Sanz, E., Jouanno, J., Chaigneau, A., Candela, J., & Tenreiro, M. (2020, 7). Erosion of the subsurface salinity maximum of the loop current eddies from glider observations and a numerical model. *Journal of Geophysical Research: Oceans*, *125*. doi: 10.1029/2019JC015397

Steele, J. H. (1964). A study of the production in the gulf of mexico. *Journal of Marine Research*, *22*, 211-222.

Stern, M. E. (1965). Interaction of a uniform wind stress with a geostrophic vortex. *Deep-Sea Research*, *12*, 355-367.

Sverdrup, H. U. (1953). On conditions for the vernal blooming of phytoplankton. *ICES Journal of Marine Science*, *18*, 287-295. doi: https://doi.org/10.1093/icesjms/18.3.287

Sánchez-Velasco, L., Lavín, M. F., Jiménez-Rosenberg, S. P. A., Godínez, V. M., del Angel, E. S., & Hernández-Becerril, D. U. (2013). Three-dimensional distribution of fish larvae in a cyclonic eddy in the gulf of california during the summer. *Deep Sea Research I*, *75*, 39-51. doi: https://doi.org/10.1016/j.dsr.2013.01.009

Taylor, J. R., & Ferrari, R. (2011, 11). Shutdown of turbulent convection as a new criterion for the onset of spring phytoplankton blooms. *Limnology and Oceanography*, *56*, 2293-2307. doi: 10.4319/lo.2011.56.6.2293

Thomalla, S. J., Moutier, W., Ryan-Keogh, T. J., Gregor, L., & Schütt, J. (2018, 2). An optimized method for correcting fluorescence quenching using optical backscattering on autonomous platforms. *Limnology and Oceanography: Methods*, *16*, 132-144. doi: 10.1002/lom3.10234

Vaillancourt, R. D., Marra, J., Seki, M. P., Parsons, M. L., & Bidigare, R. R. (2003). Impact of a cyclonic eddy on phytoplankton community structure and photosynthetic competency in the subtropical north pacific ocean. *Deep-Sea Research Part I: Oceanographic Research Papers*, *50*, 829-847. doi: 10.1016/S0967-0637(03)00059-1

Valente, A., Sathyendranath, S., Brotas, V., Groom, S., Grant, M., Taberner, M., ... Zibordi, G. (2019, 7). A compilation of global bio-optical in situ data for ocean-colour satellite applications - version two. *Earth System Science Data*, *11*, 1037-1068. doi: 10.5194/essd-11-1037-2019

Velásquez-Aristizábal, J. A., Camacho-Ibar, V. F., Durazo, R., Valencia-Gasti, J. A., Lee-Sánchez, E., & Trasviña-Castro, A. (2022). Nitracentric/hydrographic classification and prediction of nitrate profiles for oceanographic stations under the influence of mesoscale eddies in the gulf of mexico. *Frontiers in Marine Science*, *9*, 827574.

Wenegrat, J. O., & Thomas, L. N. (2017, 5). Ekman transport in balanced currents with curvature. *Journal of Physical Oceanography*, *47*, 1189-1203. doi: 10.1175/JPO-D-16-0239.1

Yang, B., Gomez, F., Schmid, C., & Baringer, M. (2022, 10). In situ estimates of net primary production in the open-ocean gulf of mexico. *Limnology And Oceanography Letters*, *7*, 427-434. doi: 10.1002/lol2.10270

Zavala-Hidalgo, J., Romero-Centeno, R., Mateos-Jasso, A., & Morey, S. L. (2014). The response of the gulf of mexico to wind and heat flux forcing: What has been learned in recent years? *Atmósfera*, *27*, 317-334. doi: 10.1016/S0187-6236(14)71119-1

Figure_01.

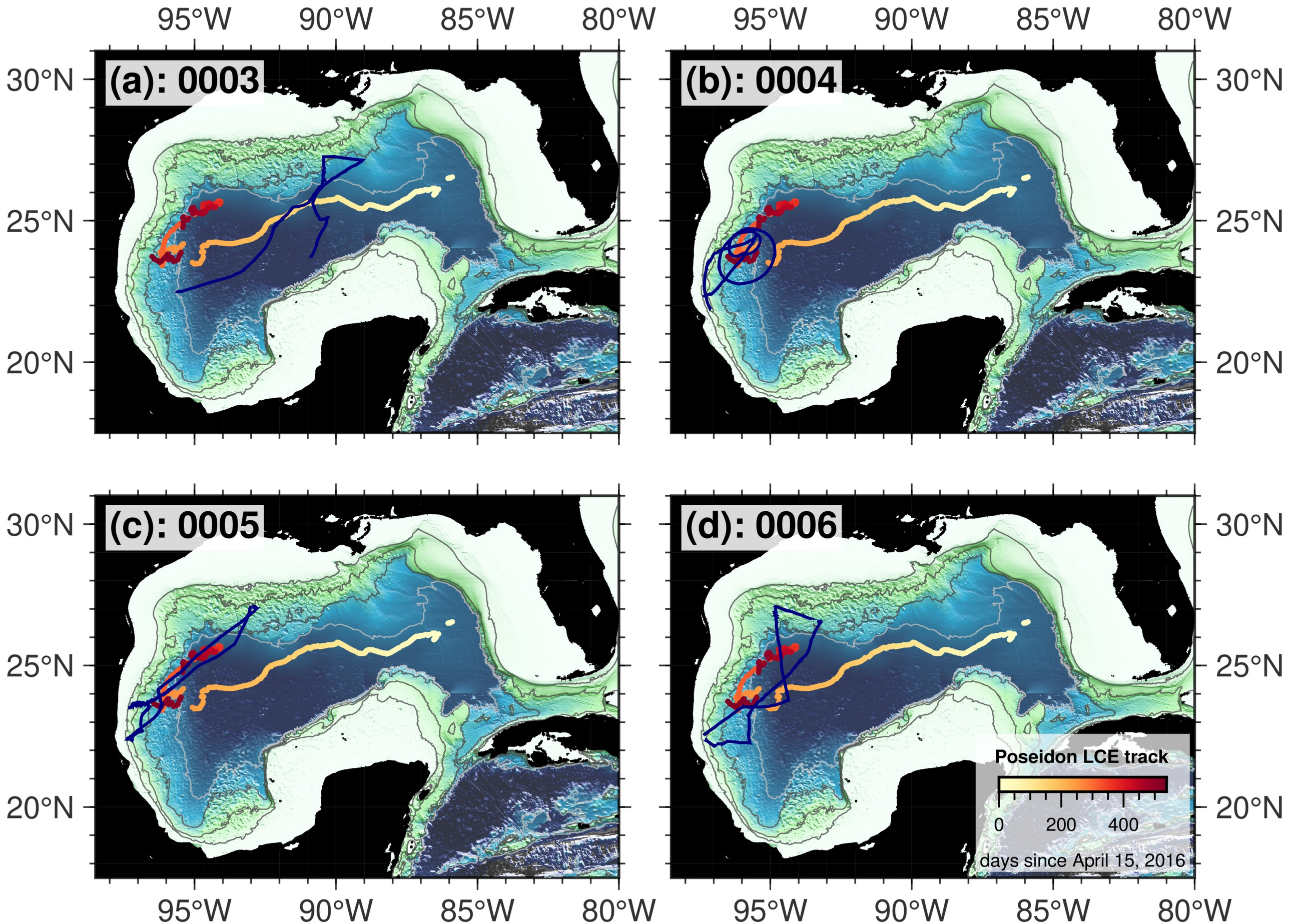
(a): 0003
(b): 0004
(c): 0005
(d): 0006
95°W
90°W
85°W
80°W
30°N
25°N
20°N
Poseidon LCE track
0
200
400
days since April 15, 2016

Figure_02.

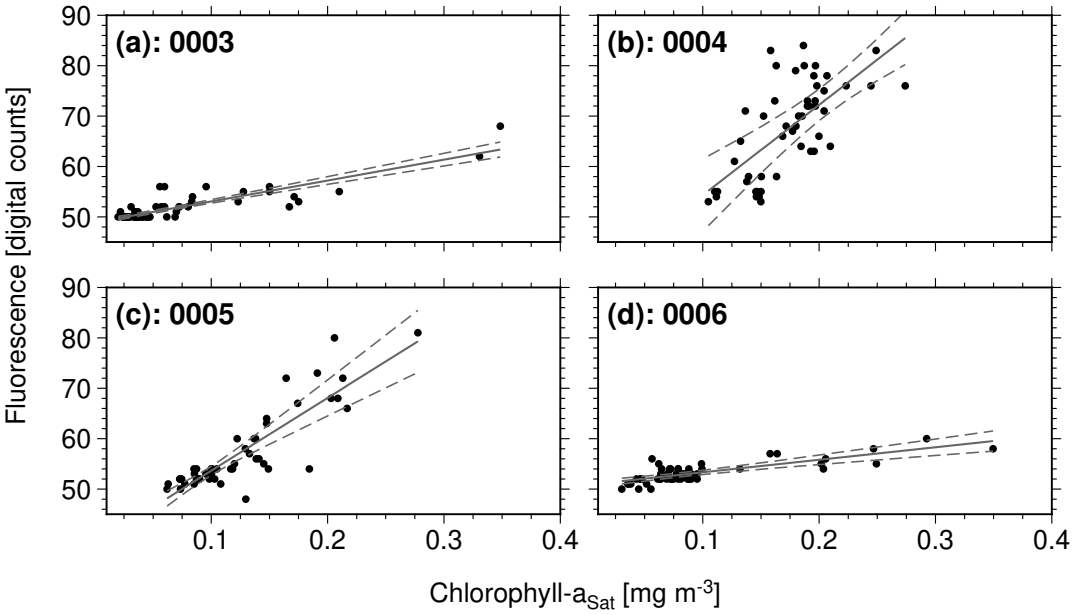
(a): 0003
(b): 0004
(c): 0005
(d): 0006
Fluorescence [digital counts]
Chlorophyll-a$_{Sat}$ [mg m^{-3}]
90
80
70
60
50
0.1
0.2
0.3
0.4

Figure_03.

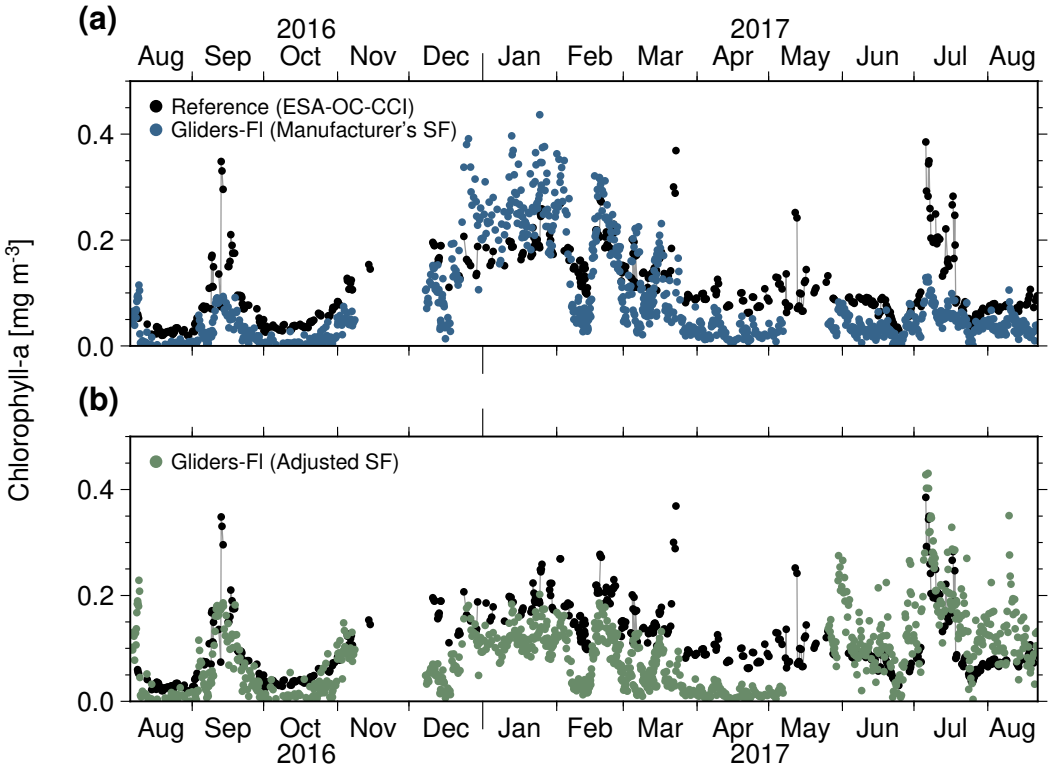
(a)
2016
2017
Aug
Sep
Oct
Nov
Dec
Jan
Feb
Mar
Apr
May
Jun
Jul
Aug
Reference (ESA-OC-CCI)
Gliders-Fl (Manufacturer's SF)
0.4
0.2
0.0
Chlorophyll-a [mg m-3]
(b)
Gliders-Fl (Adjusted SF)
0.4
0.2
0.0
Aug
Sep
Oct
Nov
Dec
Jan
Feb
Mar
Apr
May
Jun
Jul
Aug
2016
2017

Figure_04.

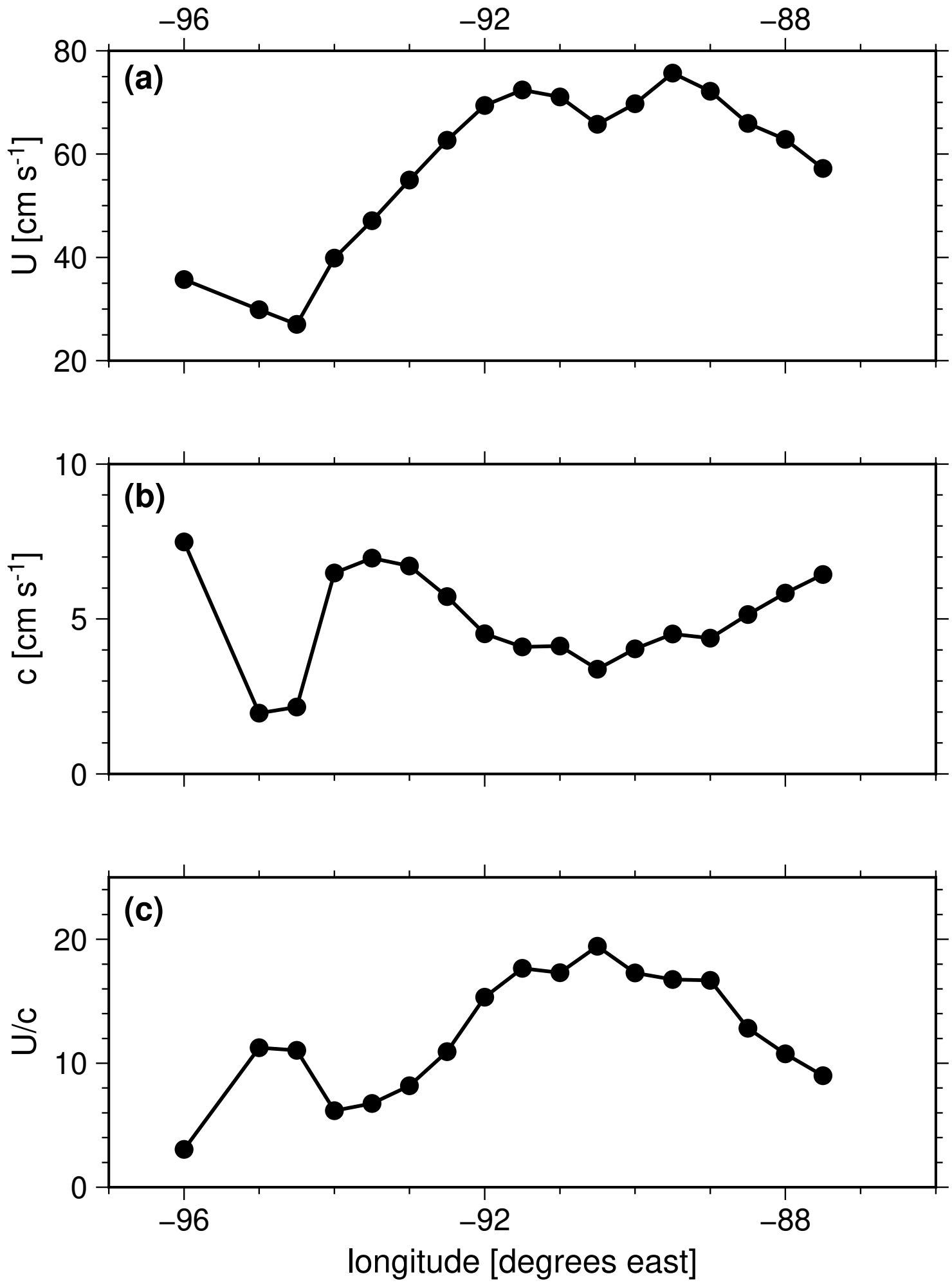
(a)
U [cm s-1]
80
60
40
20
(b)
c [cm s-1]
10
5
0
(c)
U/c
20
10
0
−96
−92
−88
longitude [degrees east]

Figure_05.

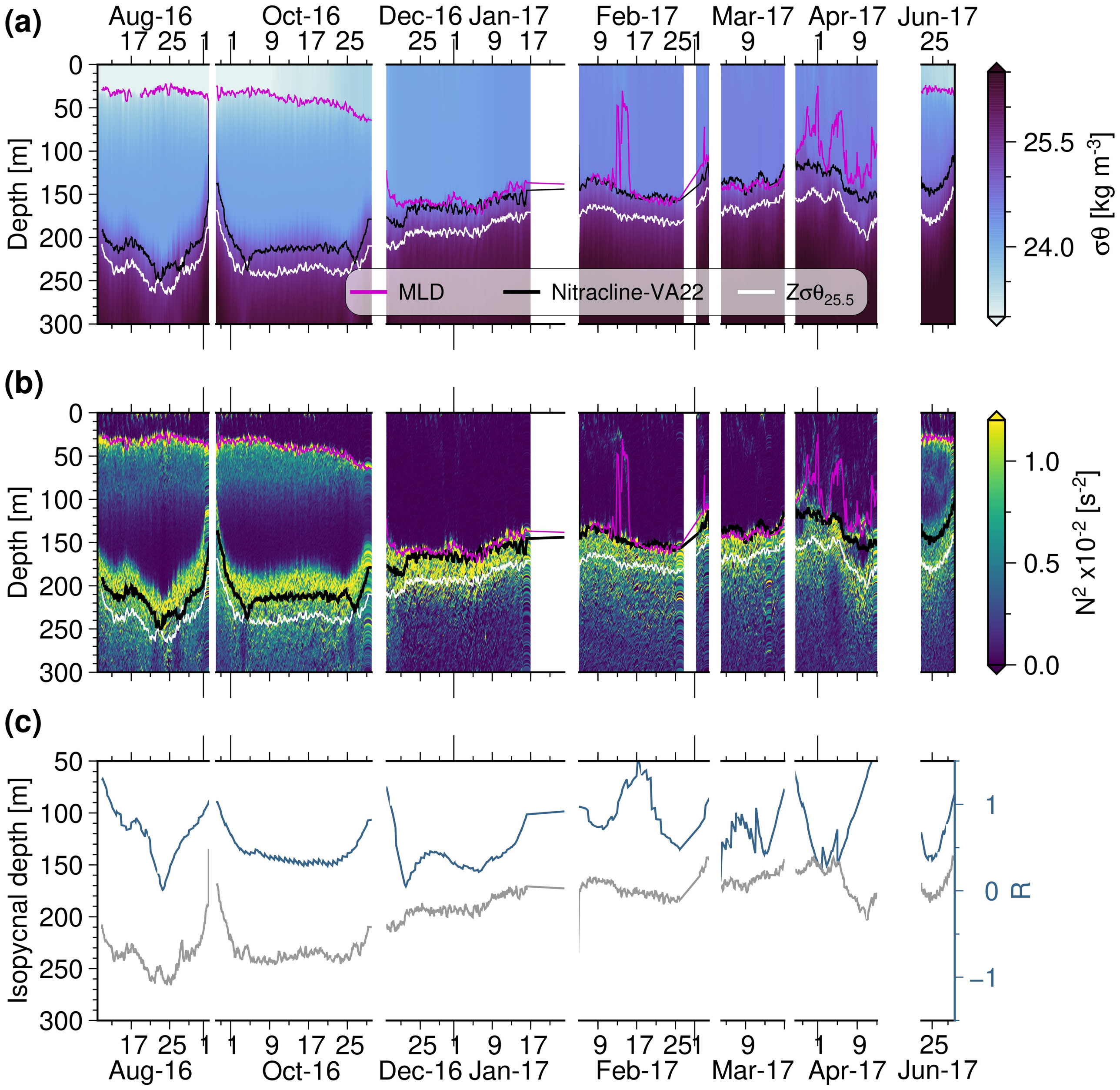
(a)
Aug-16
Oct-16
Dec-16
Jan-17
Feb-17
Mar-17
Apr-17
Jun-17
Depth [m]
MLD
Nitracline-VA22
Zσθ25.5
σθ [kg m-3]
25.5
24.0
(b)
Depth [m]
N2 x10-2 [s-2]
1.0
0.5
0.0
(c)
Isopycnal depth [m]
R

Figure_06.

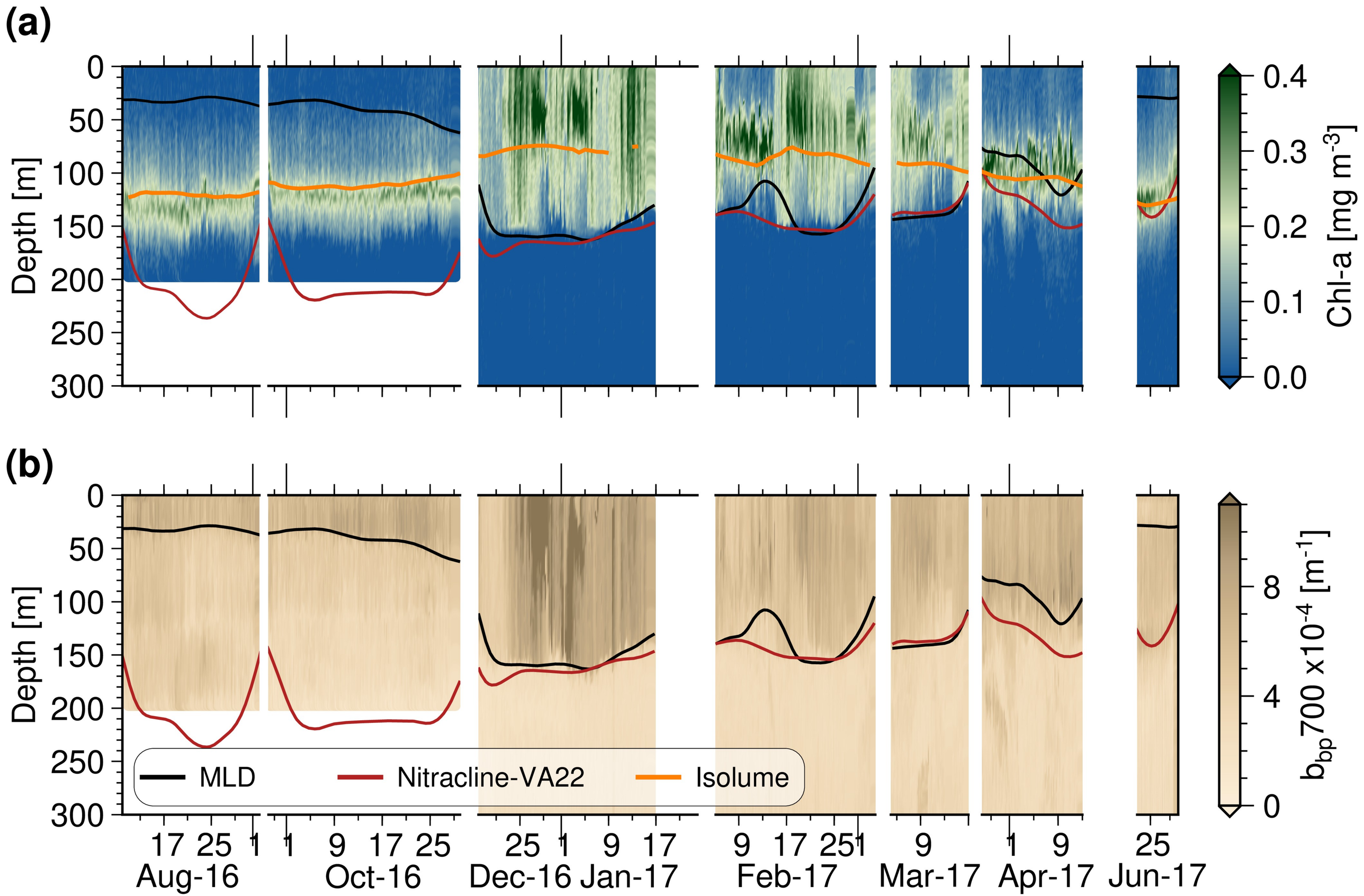
(a)
(b)
Depth [m]
0
50
100
150
200
250
300
Chl-a [mg m-3]
0.0
0.1
0.2
0.3
0.4
bbp700 x10-4 [m-1]
0
4
8
MLD
Nitracline-VA22
Isolume
17 25 1
Aug-16
1 9 17 25
Oct-16
25 1 9 17
Dec-16 Jan-17
9 17 25 1
Feb-17
9
Mar-17
1 9
Apr-17
25
Jun-17

Figure_07.

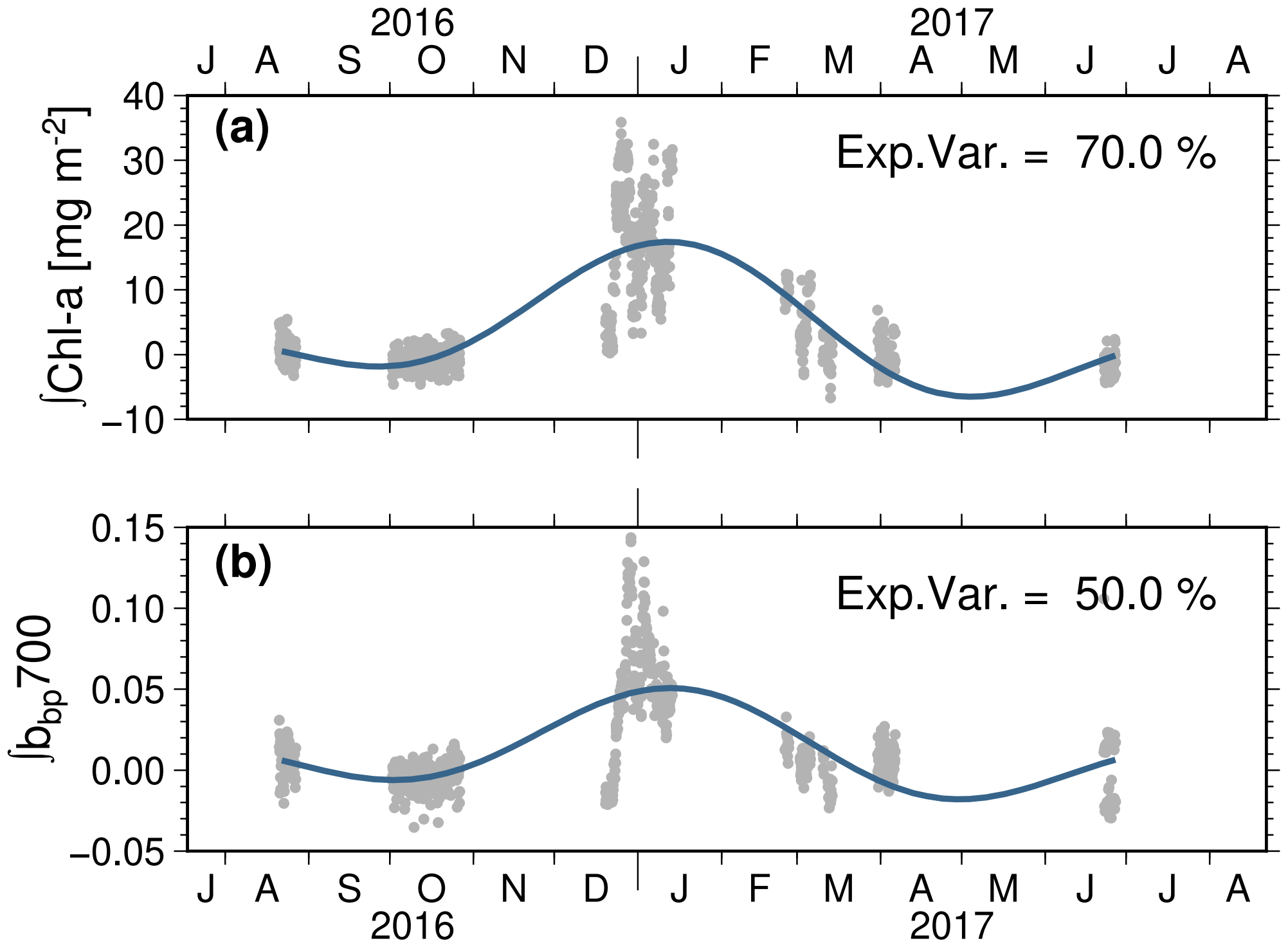
2016
2017
J A S O N D J F M A M J J A
(a)
Exp.Var. = 70.0 %
∫Chl-a [mg m-2]
40
30
20
10
0
−10
(b)
Exp.Var. = 50.0 %
∫bbp700
0.15
0.10
0.05
0.00
−0.05
J A S O N D J F M A M J J A
2016
2017

Figure_08.

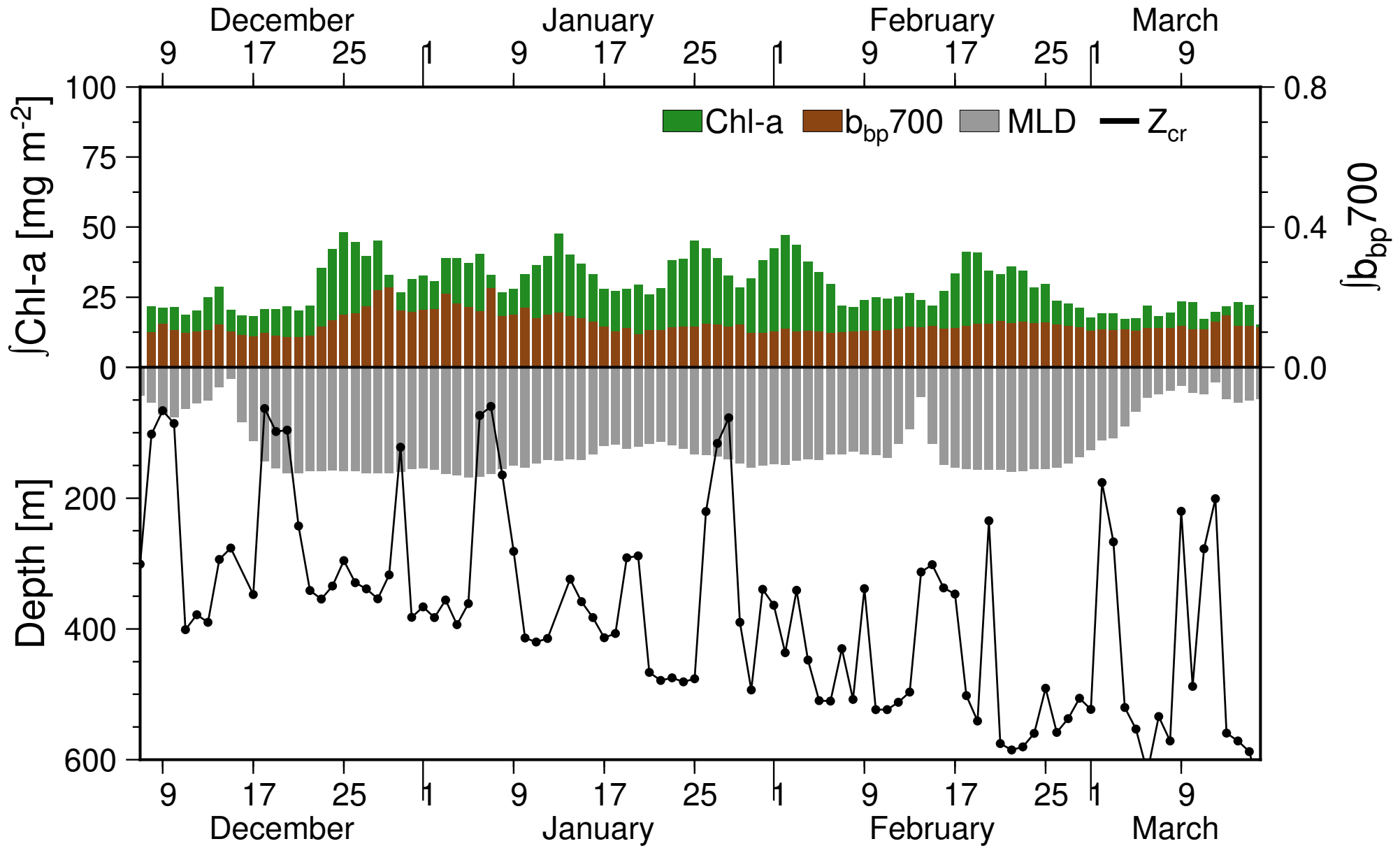
December
January
February
March
9
17
25
1
Chl-a
$b_{bp}700$
MLD
Z_{cr}
∫Chl-a [mg m^{-2}]
∫b_{bp}700
Depth [m]
100
75
50
25
0
0.8
0.4
0.0
200
400
600